Spring 5-2015

Study of Laser Speckle Scattering in Vitreous Humor Models

Wanseok Oh
Rose-Hulman Institute of Technology

Study of Laser Speckle Scattering in Vitreous Humor Models

A Thesis

Submitted to the Faculty

of

Rose-Hulman Institute of Technology

by

Wanseok Oh

In Partial Fulfillment of the Requirements for the Degree

of

Master of Science in Optical Engineering

May 2015

ROSE-HULMAN INSTITUTE OF TECHNOLOGY

Final Examination Report

Wanseok Oh — Name

Optical Engineering — Graduate Major

Thesis Title: Study of Laser Speckle Scattering in Vitreous Humor Models

DATE OF EXAM: May 7, 2015

EXAMINATION COMMITTEE:

	Thesis Advisory Committee	Department
Thesis Advisor:	Charles Joenathan	PHOE
	Robert Bunch	PHOE
	Ashley Bernal	ME

PASSED X FAILED

ABSTRACT

Oh, Wanseok

M.S.O.E

Rose-Hulman Institute of Technology

May 2015

Study of Laser Speckle Scattering in Vitreous Humor Models

Thesis Advisor: Dr. Charles Joenathan

When a highly high coherent light propagates through a medium, interactions between light and the medium produces a unique intensity speckle pattern that is dependent on several factors such as particle size in the medium, wavelength of the light, concentration of medium, and scattering angle. Speckle patterns from either static or dynamic specimens have been studied using optical techniques due to its non-invasive nature. Speckle patterns from biological specimens (dynamic) are different from that of the static specimens since random movement of molecules (Brownian motion) in the biological specimen affect the light interactions and thereby the intensity of the speckles in the speckle pattern. Several studies have shown the optical properties of the biological specimen can be characterized using statistical properties from the speckle pattern. A histogram of intensity distribution of the speckle pattern can be used to extract certain optical properties of the specimen such as bioactivity, blood flow, and skin perfusion. In this thesis, a new approach for analyzing biological specimens is presented utilizing a

peak shift in the histogram plot (called the Histogram Wavelength Analysis Method) of the intensity of the speckles when changing the wavelength of the incident light. Five different wavelengths were used in a modified slit-lamp equipment for the experiment. Also six different sizes of nanobeads embedded in vitreous humor (biological specimen) were studied. The theory developed for this experimental method matches well with the results and will be presented in the thesis

ACKNOWLEDGEMENT

There are many people who deserve recognition for their part in this thesis, but in this limited space I would like to name few of the greatest contributors.

To my beloved wife, Miran Hong, I give this as a small consolation for all you have sacrificed for our family. Your selfless devotion has been essential for the realization of this thesis. To my first son, Liam E. Oh, and my unborn son, Luke S. Oh, you have been the main source of my joy and motivation to pursue this career path. My happiness will continue to come from watching you grow up soundly.

I would like to express my deepest gratitude to my father, Seil Oh, and my mother, Jeongae Park, for their support and patience, without which I could not have finished. Also, I am truly grateful to my parents-in-law, Soonkwon Hong, and Kio Bae, for encouraging me with their best wishes. I would like to express my sincere gratitude to my grandmother-in-law, Seyoung Oh, for praying for spiritual and physical health and a promising future of my family. I would further like to thank my sister-in-law, Mihee Hong, for her devotion and sacrifice to my family.

I would like to express my special appreciation to my advisor Dr. Charles Joenathan for giving me continual guidance, unlimited enthusiasm, and immense knowledge toward completion of this work, and for his gracious understanding during his tenure as my professor. I could not have imagined a better advisor and mentor for

graduate study. I would like to thank Dr. Ashley Bernal for her willingness to serve on my advisory committee and for her tremendous time commitment in correcting and revising my thesis manuscript. I appreciate Dr. Robert M. Bunch for his service on my advisory committee and for his instruction into the theory of my research and for his discussion about my work. I would especially like to thank Dr. Nathan Ravi for engaging me an interesting fulfilling research topic. I am grateful to Paul D. Hamilton for his inclination to readily give his time and skills to help with my experiment. I would like to express warm thanks Dr. Chibum Lee and Dr. Wonjong Joo for their generous attention to my education. I would like to express my sincerest thanks to Benjamin D. Hall for his invaluable time and thoughtful behaviors to enrich my life.

I would like to acknowledge The Department of Physics and Optical Engineering at Rose-Hulman Institute of Technology and The Department of Ophthalmology and Visual Sciences at Washington University School of Medicine in St. Louis for allowing me to use its laboratory and equipment throughout this study.

May the almighty bless you with everything best in life!

TABLE OF CONTENTS

LIST OF FIGURES

LIST OF TABLES

1. INTRODUCTION

Speckle patterns are formed when an incident beam is passed through a medium with random refractive index or reflected from rough surfaces. Generally, statistical analysis has been used to understand the properties of the scattered light [1]. The intensity and phase distribution of the speckle pattern has been used to make mechanical measurements on static or dynamic objects and used to extract bioactivity of biological specimen [2-6]. Speckle patterns from living materials are different from those of inactive materials since the intensity distribution of the speckle pattern from the living materials is constantly fluctuating due to the Brownian motion of the molecules in the materials. Dynamic speckles have been used for many applications such as blood flow, chemical reactions, ophthalmology, and studying animal and plant material to name a few [7-16]. Since the scattered light is generated from stationary and moving scatterers, the contrast of the speckle pattern has been initially used to analyze bioactivity. Further, the contrast of the time average picture was used to extract information about the relative magnitude of the movement of the scatterers [7, 12]. Also a series of frames of the speckle pattern was recorded providing the time history of the motion where the brightness was related to the motion in the specimen [13]. A co-occurrence matrix method was then developed to estimate the time evolution of the speckles in the frames, thereby determining the bioactivity [14, 15]. In addition to these temporal studies, spatial

analysis has also been performed where the weighted sums of the difference between two snap shots of the speckle patterns was used to measure blood flow. This technique is called the Fujii method and was subsequently improved [16, 17]. To improve on the Fujii method, a generalized difference (GD) approach using the sum modulus value of the intensity difference was developed but these methods were shown to be computationally tedious [7, 18]. In this study the phenomena of how the light scattered from biological specimens varied with the change in wavelength were explored. To extract some useful information from a single frame of the speckle pattern, the histogram distribution of the intensity of the speckles was used. In the experiment, a rectangular beam illuminated the biological specimen which is a vitreous humor substitute. The resulting scattered beam was collected and the histogram distribution of the speckle intensity at the image plane was analyzed.

The histogram of the intensity of the speckle pattern was normalized to compare the distribution from samples with various peak shift at one specific angle of illumination and observation angle. In the experiment, five different wavelengths from different laser diodes were exactly positioned at the same location while maintaining the beam profile and intensity. Also six different sizes of nanobead suspended in vitreous humor substitute were studied. Speckle pattern images recorded by CCD camera were then imported to Matlab software to perform the required mathematical analysis on each image. The histogram is calculated by sorting the intensity pixel numbers as a function of intensity

value from 0 to 255. The values are normalized and then plotted. It was found that the profiles of the histograms were identical, but the peaks were found to shift with the change in the wavelength of the illuminating beam and with the change in the nanobead size. The histogram peak shift as a function of wavelength method is called the Histogram Wavelength Analysis Method (HWAM). Relationships between nanobead size in vitreous humor substitute and laser wavelength were determined using HWAM. The shift as a function of wavelength is related to the nanobead size less than 200 nm and for nanobead sizes above 200 nm size the curves overlap with each other thus making it difficult to differentiate different nanobead size. In this thesis, both the theoretical and experimental results of this fundamental study are presented.

2. BACKGROUND

2.1 Speckle Theory

When a highly coherent light such as laser is incident on a rough surface or propagates through a medium with random refractive index, the light is scattered in all directions. This scattered light interferes with itself and causes a random interference pattern called a speckle pattern. Speckle patterns, consisting of bright and dark patterns, arise due to the summed phase (phase shift) and amplitude of the scattered light. As the scattered beam has varying optical path length difference, bright spots are produced when the rays are in-phase, whereas dark spots are produced when the rays are out-of-phase. Since the surface is random, the intensity distribution is also random both in space and in the temporal domain. One such speckle pattern image used in this thesis is shown in Figure 1.

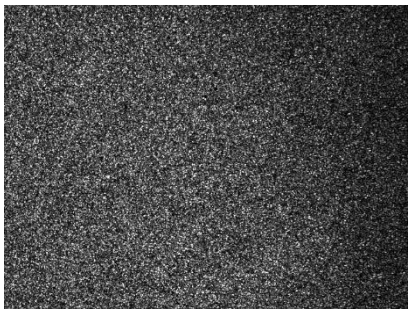

Figure 1. Photograph of a speckle pattern image. (400 nm nanobead is embedded in 0.4 wt% biological specimen, the incident wavelength is 405 nm and scattering angle is 30°)

Speckle pattern phenomena have been investigated since the time of Newton and was sketched by Karl Exner in 1877 [5, 19, 20]. Initially, when speckle patterns were investigated by researchers and scientists, they were considered to be a nuisance effect in images since their granularity degraded the resolution of the images [6, 21-24]. Therefore, many studies have been focused on enhancing the quality of the image by suppressing the speckle patterns in the image [1, 25-29]. However, speckle phenomena were revisited after the invention of laser during the 1960s [1, 4, 5, 12, 24, 30]. It has been demonstrated that the statistical properties of speckle patterns, which are generated by the interactions between the medium and light, are directly related to the medium [1-3, 7, 9, 12, 18, 24, 25, 31, 32]. For instance, speckle patterns from static objects are different from those of dynamic objects. Speckle theory was developed in the 1960s, and the speckle was used for measurement of displacements [21, 33-36].

The first statistical analysis of the speckle pattern was described by Lord Rayleigh in a series of papers starting in 1880, and the comprehensive mathematical description was fully developed following x-ray scattering theory [31, 32]. The statistical analysis of the speckle pattern was feasible since the optical properties of the specimen are related to the optical properties of the scattered light. The temporal and spatial contrast of speckle patterns has been employed to provide information about the physical properties of the specimen [37-45]. The 1^{st} order statistics of speckle pattern describe the properties of the speckle pattern point by point whereas 2^{nd} order statistics of the speckle pattern describe

the properties of the speckle pattern using the speed of intensity variations from point to point in the speckle pattern image [2].

In the 1st order statistics, the ratio of the standard deviation of the intensity to the mean intensity value is an important parameter since it is used to determine the contrast of the speckle pattern. The complex amplitude of speckle light field at an observing plane (x, y, z) in a speckle pattern image can be expressed as the sum of scattered light from the medium. The complex amplitude of the speckle light field is calculated using all scattered light arriving for all points on the scattering object. The complex amplitude of the speckle light field, $A(x, y, z)$, at some observation plane can be expressed as [31, 32, 46-48]

$$A(x, y, z) = \frac{1}{\sqrt{N}} \sum_{K=1}^{N} A_k exp(j\emptyset_k) \quad (1)$$

where N is the number of scatterers, A_k is the random amplitude of the k^{th} element from the medium, and $\emptyset_k$ is the random phase of the k^{th} element from the medium. In the complex amplitude of the speckle light field description it is assumed that monochromatic light is reflected from or transmitted through a rough medium. The following assumptions are used to develop the first order statistics for speckles [31, 32, 48].

i. The scatterers are randomly distributed with uniform probability.

ii. The amplitude, A_k, of the k^{th} contribution are statistically independent random variables.

iii. The phase, $\emptyset_k$, of the k^{th} contribution are statistically independent random variables.

iv. The amplitude, A_k, of the k^{th} contribution and the phase, $\emptyset_k$, of the k^{th} contribution are statistically independent between them.

v. The phase, $\emptyset_k$, of the k^{th} contribution are uniformly distributed over $[-\pi; +\pi]$.

A rough surface approximation, which requires the height variation of the surface to be greater than wavelength of light, is employed to validate assumption v. The complex amplitude of the speckle light field obeys Gaussian statistics according to the central limit theorem. The probability density function (PDF) for the real and imaginary part of the complex amplitude of the speckle light field is given by [32, 46-48]

$$PDF(A_r, A_i) = \frac{1}{2\pi\sigma^2} exp\left\{-\frac{A_r^2 + A_i^2}{2\sigma^2}\right\} \quad (2)$$

where A_r is a real part of the complex amplitude of the speckle light field, A_i is an imaginary part of the complex amplitude of the speckle light field, and σ^2 is a variance which is given by

$$\sigma^2 = \lim_{n\to\infty} \frac{1}{N} \sum_{K=1}^{N} \frac{\langle |A_k|^2 \rangle}{2} \tag{3}$$

where $\langle\ \rangle$ means the ensemble average. The complex amplitude of the speckle light field obeys Gaussian statistics under two conditions; the phase of the scattered light field at the scatterer is uniform over $-\pi;\ +\pi$, and $N \to \infty$. The complex amplitude of the speckle light field will show a complex circular Gaussian distribution. The probability density function of the intensity of the scattered light, $PDF(I)$, can be written as [32, 46-48]

$$PDF(I) = \frac{1}{2\sigma^2} exp\left(-\frac{I}{2\sigma^2}\right) \tag{4}$$

The absolute intensity value of the scattered light will decrease exponentially when the intensity is detected by a CCD camera. Thus the probability density function of the detected intensity, $PDF(I_d)$, can be written as [32, 46-48]

$$PDF(I_d) = \left(\frac{n_0}{\langle I \rangle}\right)^{n_0} \frac{I_d^{n_0-1}}{\Gamma(n_0)} exp\left(-\frac{n_0 I_d}{\langle I \rangle}\right) \tag{5}$$

where n_0 can be interpreted as the number of speckle grains which are detected by a CCD camera and Γ is Gamma function. The probability density function of the detected intensity, $PDF(I_d)$, is apt to follow Gaussian distribution when $n_0 \to \infty$.

In the 2nd order statistics, the size of the speckle and distribution of the speckle size are derived since it describes the intensity variations in the speckle pattern image.

The Power Spectral Density (PSD) of a signal is defined by the modulus squared of its Fourier transform (FT). The PSD of the detected intensity is written as [48]

$$PSD(I(x,y)) = |FT(I(x,y))|^2 \tag{6}$$

The autocorrelation function, R_1, of the intensity at two arbitrary points (x_1, y_1), (x_2, y_2) in the observation plane is defined as [32, 48]

$$R_1(\Delta x, \Delta y) = \langle I(x_1, y_1) I(x_2, y_2) \rangle \tag{7}$$

where $\Delta x = x_1 - x_2$ and $\Delta y = y_1 - y_2$. If $x_2 = 0$ and $y_2 = 0$, the autocorrelation function is written as [32, 48]

$$R_1(\Delta x, \Delta y) = R_1(x, y) \tag{8}$$

According to the Wiener-Khintchine theorem, the autocorrelation function of the intensity is given by the Inverse Fourier Transform (FT^{-1}) of the PSD of the intensity which is written as [32, 48]

$$R_1(x,y) = FT^{-1}[PSD(I(x,y))] \tag{9}$$

The normalized auto covariance function of the intensity ($c_I(x,y)$) corresponds to the normalized autocorrelation function with a zero base and provides a reasonable measurement of the average width of a speckle [32, 48]

$$C_I(x,y) = \frac{R_1(x,y) - \langle I(x,y)\rangle^2}{\langle I(x,y)^2\rangle - \langle I(x,y)\rangle^2} \quad (10)$$

The normalized auto covariance function of the intensity can be calculated from the intensity distribution of the measured speckle [32, 48]

$$C_I(x,y) = \frac{FT^{-1}(|FT(I(x,y))|^2) - \langle I(x,y)\rangle^2}{\langle I(x,y)^2\rangle - \langle I(x,y)\rangle^2} \quad (11)$$

$C_I(x,0)$ and $C_I(y,0)$ correspond to the horizontal and the vertical profiles of $C_I(x,y)$, respectively. Their width at half maximum are denoted *dx* and *dy*, respectively.

2.2 Speckle Contrast

In biological specimens, movement of the particles leads to speckle pattern variations in time so spatial contrast of the speckle pattern will decrease due to Doppler effects [4, 12, 24, 39, 43]. Fundamental speckle contrast theory has been introduced and several studies have employed a laser speckle contrast technique for blood flow and tissue perfusion analysis [24, 37-45, 49-51]. There are many techniques which uses speckle contrast and the names are different depending on domains and principles [39]. One of the techniques is called Laser Speckle Contrast Imaging (LSCI) which was introduced in the 1980s. This technique has been used for clinical purposes due to the availability of faster acquisition devices and new image processing techniques [4, 37, 52-57]. LSCI is based on the changes of a speckle pattern over time since the biological

material is constantly moving. The movement of active scatterers can be quantified and analyzed either by its temporal variations or by its spatial variations. Speckle contrast studies using spatial or the temporal statistics have been utilized for the study of blood flow [4, 24]. Speckle de-correlation time is long (on the order of milliseconds) compared to the typical de-correlation time, so the recorded speckle pattern image is blurred [39, 58, 59]. The blurred speckle pattern image is quantified by the spatial speckle contrast, K_s, which is written as

$$K_s = \frac{\sigma_s}{\langle I \rangle} = \frac{\sqrt{\langle I^2 \rangle - \langle I \rangle^2}}{\langle I \rangle} \tag{12}$$

where σ_s is the spatial standard deviation of the intensity and $\langle I \rangle$ is the mean intensity of the speckle pattern. Similarly, the temporal speckle pattern is denoted C_t, and temporal standard deviation is denoted σ_t. There is no doubt that the contrast of the speckle pattern image is fluctuating which is dependent on the movement of scatterers in the medium. Thus, it can be analyzed either spatially or temporally. Theoretically, the speckle contrast value is ranging from 0 to 1. If the spatial speckle contrast is 1, there is no movement on the speckle pattern. If the spatial speckle contrast is 0, the movement of scatterers are very fast and blur the speckle images. The speckle contrast is a function of the exposure time, T, of a CCD camera and is related to the autocovariance, $C_t(\tau)$, of the intensity fluctuations in a single speckle which is written as

$$K^2 = \frac{\sigma_s^2(T)}{\langle I \rangle^2} = \frac{1}{T\langle I \rangle^2} \int_0^T C_t(\tau) d\tau \tag{13}$$

where the autocovariance, $C_t(\tau)$, is written as

$$C_t(\tau) = \langle [I(t) - \langle I \rangle_t][I(t+\tau) - \langle I \rangle_t] \rangle_t \tag{14}$$

where $\langle\ \rangle_t$ is the time-averaged quantity, and τ is the correlation time. The relationship between the autocovariance, $C_t(\tau)$, and the intensity correlation function, $g_2(\tau)$, is written as

$$g_2(\tau) = 1 + \frac{C_t(\tau)}{\langle I \rangle_t^2} \tag{15}$$

The Siegert Equation relates the electric field correlation function, $g_1(\tau)$, and the intensity correlation function, $g_2(\tau)$, which is written as

$$g_2(\tau) = 1 + \beta [g_1(\tau)]^2 \tag{16}$$

where β is a correction factor which is affected by the experimental setup. It is common to assume that the electric field correlation function, $g_1(\tau)$, is written as

$$g_1(\tau) = exp\left(-\frac{\tau}{\tau_c}\right) \tag{17}$$

where τ_c is a correlation time that is inversely proportional to the local velocity of the scatterers. Thus, speckle contrast can be written as

$$K = \beta^{0.5}\left\{\frac{\tau_c}{T} + \frac{\tau_c^2}{2T^2}\left[exp\left(-\frac{2T}{\tau_c}\right) - 1\right]\right\}^{0.5} \quad (18)$$

The speckle contrast is a function of the exposure time, T, of a CCD camera and the correlation time, τ_c,.

3. THEORY

Light scattering phenomena have been considered as the redirection of radiation from the original propagation direction when an electromagnetic wave is incident on scattering media. Light scattering techniques have been utilized for observing the dynamic phenomena in several areas including physics, chemistry, biology and medicine [60, 61, 62]. One of the main advantages of using this technique for analysis is that it is possible for real-time diagnosis. Also, it can be used either *in vivo* or *in vitro*. [63]. Light scattering theory has been employed to characterize biological specimens due to their strong optical scattering and weak absorption at wavelengths ranging from 400 nm to 1350 nm (UV, visible and near-IR) [64]. Alhazen is considered to have made the first attempt to explain interactions between light and matter in the early 11^{th} century [65].

Conventionally light scattering phenomena by spherical particles have been explained with Mie Scattering and Rayleigh scattering theory [61]. Incident light is modeled as an oscillating electromagnetic wave and once the electromagnetic wave is incident on the scattering media, the particles oscillate with the same frequency as the incident light due to the negatively charged electrons in the particles. Then, the particles are oscillating similarly to an electric dipole after interactions between the electromagnetic wave and the particles, and the frequency of the electric dipole reradiate electromagnetic waves with same frequency as the incident light [65]. If the particles are

distributed (where the mean free path between molecules is larger than both the size of a molecule and wavelength of the light), then single scattering theory is applied. However, if the molecules are distributed such that the mean free path between molecules is smaller than both the size of a molecule and the wavelength of the light, then multiple scattering events occur. Single scattering theory isn't appropriate to explain the multiple scattering phenomena since the successive independent scattering and multiple scattering are different in terms of the number of scattering events [64]. Single scattering prevails in optically thin media when photons are scattered once whereas multiple scattering prevails in optically thick media when photons are scattered more than once.

Both Rayleigh and Mie scattering theories apply to the scattering events when a light is incident on the specimen with spherical particles, but the usages of two theories are slightly different in terms of the size. Rayleigh scattering theory is applicable to small spherical particles such as atoms and molecules, and Mie scattering theory expresses a generalized scattering phenomenon by a spherical particle which is homogeneous, isotropic, and any size [64, 66]. Specific scattering regimes are required to discriminate Rayleigh and Mie scattering. A non-dimensional parameter, x, is called the particle size parameter and is given by

$$x = \frac{2r_s\pi}{\lambda_m} \tag{19}$$

where, r_s is the radius of a spherical particle and λ_m is the wavelength in the medium.

When the particle size parameter is much less than one, $x \ll 1$, Rayleigh scattering theory can be applied. When the particle size parameter is approximately equal to one, $x \sim 1$, Mie scattering theory can be applied. When the particle size parameter is much greater than one, $x \gg 1$, Geometric scattering theory can be applied. Table 1 shows scattering regimes depending on the particle size parameter x.

Table 1. Scattering regimes depending on the particle size parameter x.

$x \ll 1$	**Rayleigh Scattering**
$x \sim 1$	**Mie Scattering**
$x \gg 1$	**Geometric Scattering**

Mie scattering theory describes the majority of scattering events by spherical particles, and the analysis methods differ from Rayleigh scattering theory. Rayleigh scattering theory employs a simple mathematical equation whereas Mie scattering theory uses Maxwell's equations. In addition, Mie scattering theory is barely dependent on the wavelength of the light [64].

Figure 2 shows scattering events in spherical polar coordinates (r, θ, Φ) when the light is incident on a single scattering particle; r is the observation distance from the particle, θ is the polar angle (scattering angle), and Φ is the azimuthal angle. When an unpolarized incident light encounters the center of the particle (located at the origin)

where the size is smaller than the wavelength of the light, irradiance of the scattered light, I_s, is given by

$$I_s(r,\theta) = \frac{(1+\cos^2\theta)k^4|\alpha|^2}{2r^2} I_0 \tag{20}$$

where, I_s is the intensity of the scattered light, I_0 is the intensity of the unpolarized incident light, α is the polarizability of the particle, and k is the propagation constant in the background medium which is given by,

$$k = \frac{2\Delta n\pi}{\lambda} \tag{21}$$

where Δn is the refractive index difference between the polymer and the nanobead, and λ is the wavelength of the light in the vacuum. The intensity is inversely proportional to the wavelength of light and by substituting Equation 21 into Equation 20 assuming all the other variables are held constant except for wavelength,

$$I_s(r,\theta) \propto \frac{1}{\lambda^4} \tag{22}$$

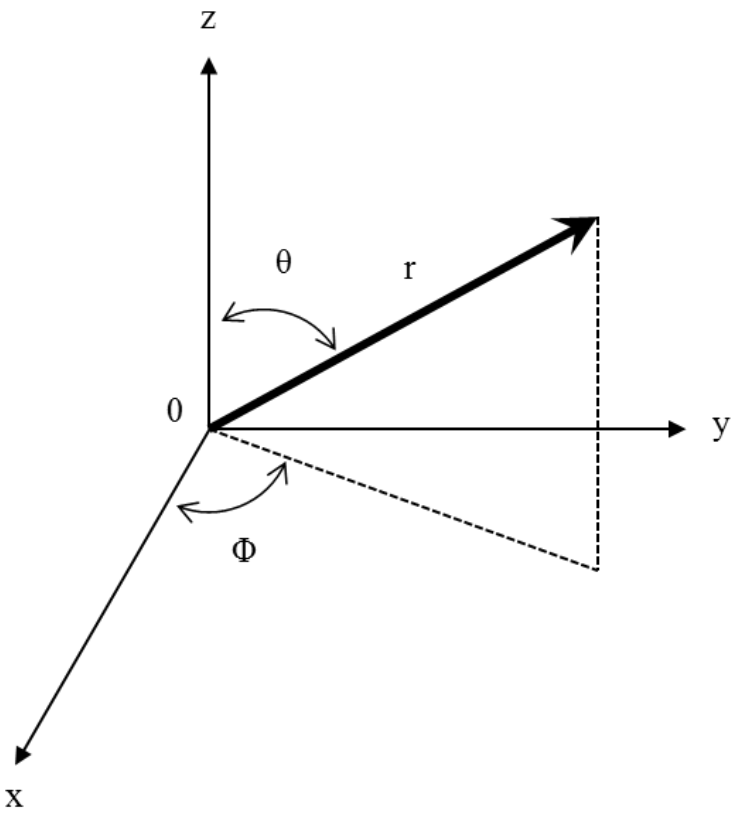

Figure 2. Schematic of light scattering events in spherical polar coordinates

Therefore, in Rayleigh scattering the intensity of the scattered light has strong dependence on the wavelength of the light and increases as the propagation constant increases. The intensity of the scattered light is the same in the forward and backward directions. Mie scattering theory is barely dependent on the wavelength of the light, and the intensity of the scattered light in forward direction is larger than in backward

direction [64]

In order to create a mathematical model, it assumed that both Mie and Rayleigh scattering occur in a biological specimen, and it is dominantly single scattering. However, light in reality can be scattered in multiple ways within the specimen. It is proposed that the scattered light from the specimen is a combination of Rayleigh and Mie scattering such that the intensity of the light can be assumed to be proportional to

$$\Delta X(I_{max}(r,\theta)) \propto c_1\left[\frac{A_1}{\lambda^4}\right] + c_2\left[\frac{A_2}{\lambda}\right] \tag{23}$$

where, $\Delta X\left(I_{max}(r,\theta)\right)$ is the histogram peak of the scattered light, c_1 and c_2 are coefficients, and A_1 and A_2 are parameters whose units are m^4 and m, respectively. Coefficients of c_1 and c_2 are non-dimensional units and are used to designate the ratio of Rayleigh scattering versus Mie scattering. In this model, it is assumed that the refractive index difference between the polymer and the embedded nanobead remain constant. Thus the refractive index variation is not included, since the light scattered by the nanobeads is collected.

The intensity of the scattered light is dependent on both the wavelength of the light and the coefficients c_1 and c_2. Theoretically, the number of speckles with the highest intensity in the speckle pattern decreases when the wavelength of the light is increased and also when the coefficient of c_1 is increased and c_2 is decreased. The

proposed Equation 23 is applied to the results from the specimen where the size of nanobead is larger than 200 nm. Table 2 shows coefficient values for normalized intensity values, and different coefficient values for the wavelength of light. Table 2a is a table of coefficients c_1 and c_2, which are applied to Equation 23 for calculation, Table 2b is a table of the normalized intensity values with respect to the wavelengths, and coefficient values c_1 and c_2 using Equation 23. Figure 3 shows plots of the shifts using the normalized scattered shifts values from Table 2.

Table 2. Coefficient values for normalized intensity values, and different coefficient values for the wavelength of light; 'a' is a table of coefficients c_1 and c_2, which are applied to Equation 23 for calculation, 'b' is a table of the normalized intensity values with respect to the wavelengths and coefficient values c_1 and c_2 using Equation 23.

	c_1	c_2
A	0.9	0.1
B	0.8	0.2
C	0.7	0.3
D	0.6	0.4
E	0.5	0.5
F	0.4	0.6
G	0.3	0.7
H	0.2	0.8
I	0.1	0.9

a

	$405nm$	$520nm$	$635nm$	$780nm$
A	1	0.40905	0.21270	0.11734
B	1	0.45014	0.25994	0.16199
C	1	0.49123	0.30717	0.20665
D	1	0.53232	0.35440	0.25130
E	1	0.57341	0.40163	0.29596
F	1	0.61449	0.44887	0.34061
G	1	0.65558	0.49610	0.38527
H	1	0.69667	0.54333	0.42992
I	1	0.73776	0.59056	0.47458

b

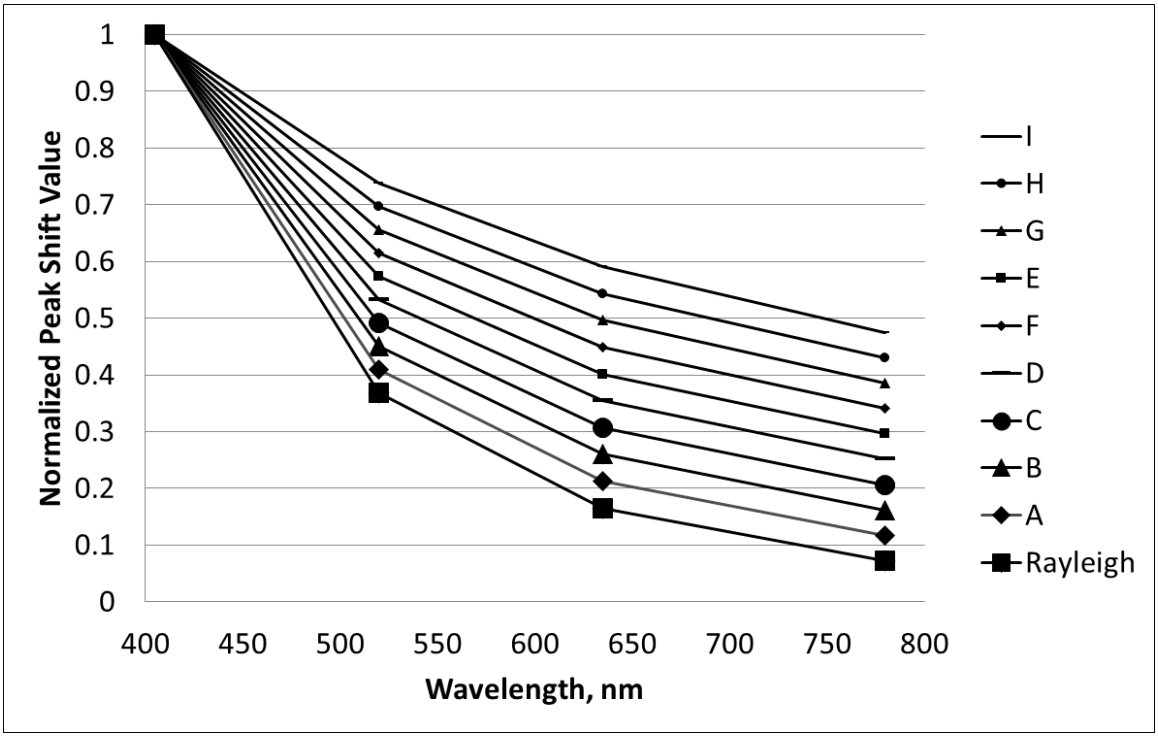

Figure 3. Diagram of theoretical normalized peak point shift with respect to the wavelength of light and coefficient values c_1 and c_2. The plots are the results of the proposed Equation 23 and coefficient values in Table 2.

To explain the angle dependency of the intensity of the scattered light, the mathematical expression can be derived from Equation 20 assuming all other variables are held constant except for the angle. The intensity of the scattered light is proportional to the scattering angle and is given by,

$$I_s(r,\theta) \propto \cos^2\theta \tag{24}$$

where θ is the scattering angle (which is an angle between the incident light and the observation location). Here, the scattering angle, θ, is perpendicular to the propagation direction and is illustrated in Figure 2. The intensity of the scattered light varies with respect to the scattering angle and is shown in Figure 4. Equation 24 shows that the intensity value decreases with an increase in the scattering angle, which is based on Rayleigh scattering theory. Variations in the intensity of the scattered light could exist depending on several factors in the experimental environment such as particle sizes in the samples, the wavelengths of light, and the polarization of the incident light. A study showed the angle dependency of the speckle pattern by comparing speckle contrast values with the scattering angles in LCD screens [68].

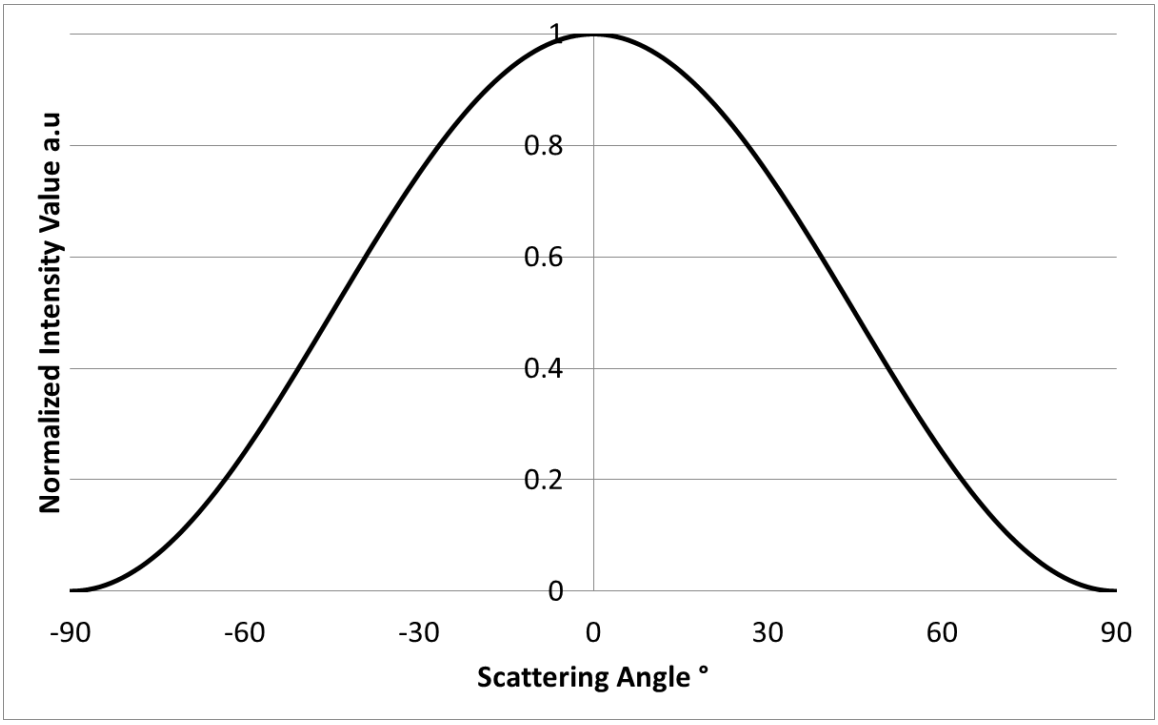

Figure 4. Diagram of the scattered intensity variations with the scattering angle ranging from -90° to 90°

Note that Equation 24 is introduced to express the intensity of the scattered light dependency on the scattering angle, and is only applicable for the single scattering phenomena by polarized light in Rayleigh scattering regimes. There many factors that affect the scattering events but the scattering angle is the only parameter in Equation 24.

Developed theory and experimental results indicated some general scattering phenomena such as a) the intensity of the scattered light from large particle scatterers is

stronger compared to small particle scatterers, and b) large particle scatterers have lower frequency than small particle scatterers [65]. Equation 20, which explains Rayleigh scattering theory, describes the scattering phenomena by one small spherical particle and can be expressed as,

$$I_s(r,\theta) = \frac{(1+\cos^2\theta)k^4}{2r^2} \cdot \left(\frac{n^2-1}{n^2+2}\right)^2 \cdot (r_s)^6 \cdot I_0 \tag{25}$$

where r_s is the radius of a spherical particle. The intensity of the scattered light is proportional to the diameter of the spherical particle which is given by,

$$I_s(r,\theta) \propto \left(\frac{r_s}{2}\right)^6 \tag{26}$$

It is assumed that the other parameters are constant except the diameter of the spherical particle. Equation 26 is introduced to explain the scattering dependency of the size variations. The intensity variation of the scattered light along with the particle size is shown in Figure 5. An assumption is made that the particle size for this study does not exceed 400 nm and this is taking as an upper limit. Five graphs show the normalized value of the intensity variations as a function of particle sizes. Several studies have shown that the intensity of the scattered light increases with an increase in the particle size [65, 66, 68-70].

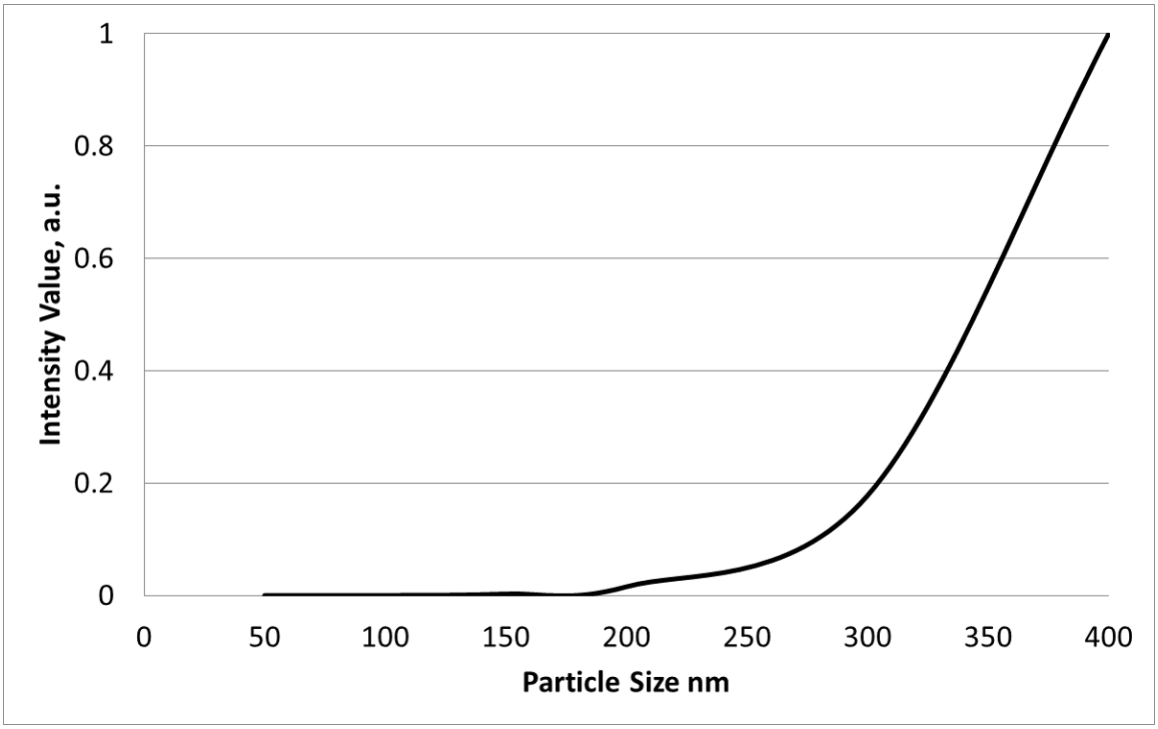

Figure 5. The diagram of the intensity variation of the scattered light with increase in the particle sizes

It should be noted that Equation 26 is utilized to express only the intensity of the scattered light dependency on the particle size of the spherical scatterer, which is for a single scattering phenomena by polarized light in Rayleigh scattering regimes.

As Rayleigh scattering theory contains the refractive index value, the relationship between the intensity of the scattered light and the refractive index value can be demonstrated. When the propagation constant, k, is applied to Equation 20, the

relationship between the intensity of the scattered light and the refractive index value is given by,

$$I_s(r, \theta) \propto \Delta n^4 \tag{27}$$

It is assumed that the other parameters are constant except refractive index. The intensity of the scattered light is proportional to the fourth power of the difference in refractive index between polymer and the nanobead and is shown in Figure 6. In the experiment, as the wavelength increases, the refractive index of both the polymer and the nanobead increase proportionally. Thus the change in refractive index remains constant.

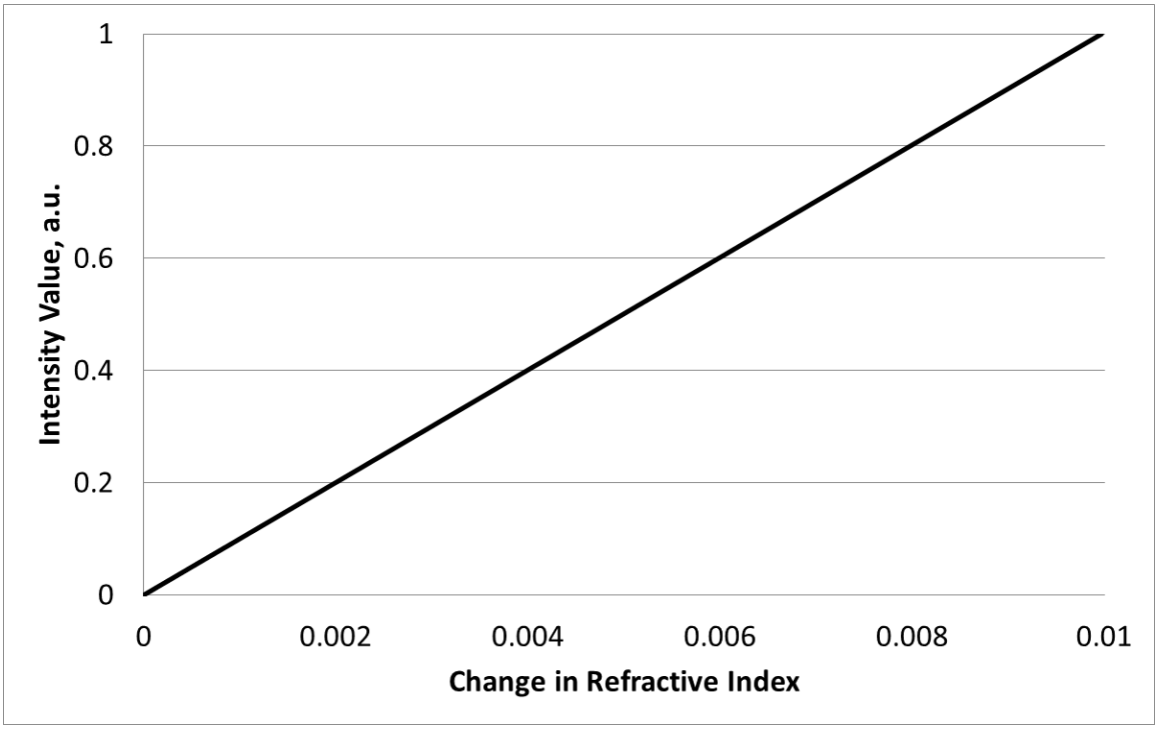

Figure 6. The diagram of the intensity variation of the scattered light with increase in the refractive index (refractive index values of polymers are acquired in Scientific Polymer Products, INC. and refractive index values of polystyrene (when the wavelength is 405 nm) are acquired in refractiveindex.info)

To explain Rayleigh scattering for polymer molecules, the intensity of the scattered light is given by,

$$I_s(r,\theta) = \frac{2\pi^2}{N_A r^2 \lambda^2} \cdot \left(\frac{d(n/n_0)}{dc}\right)^2 \cdot (1+\cos^2\theta) \cdot P(\theta) \cdot M \cdot C \cdot I_0 \tag{28}$$

where N_A is the Avogadro's number, $d(n/n_0)/dc$ is the parameter that describes the dependency of the relative refractive index of the solution on the polymer concentration (which is a measure of the polarizability of the polymer molecules), $P(\theta)$ is the size-shape factor, M is the molecular mass of the dissolved polymer molecules, and C is the concentration. Previous studies have demonstrated that the concentration dependency can be studied using Rayleigh scattering theory [65, 71, 72]. As predicted by Equation 28, the intensity of the scattered light is proportional to the concentration which is given by,

$$I_s(r, \theta) \propto C \tag{29}$$

It is assumed that the other parameters are constant except the concentration. Concentration corresponds to the intensity of the scattered light and is shown in Figure 7.

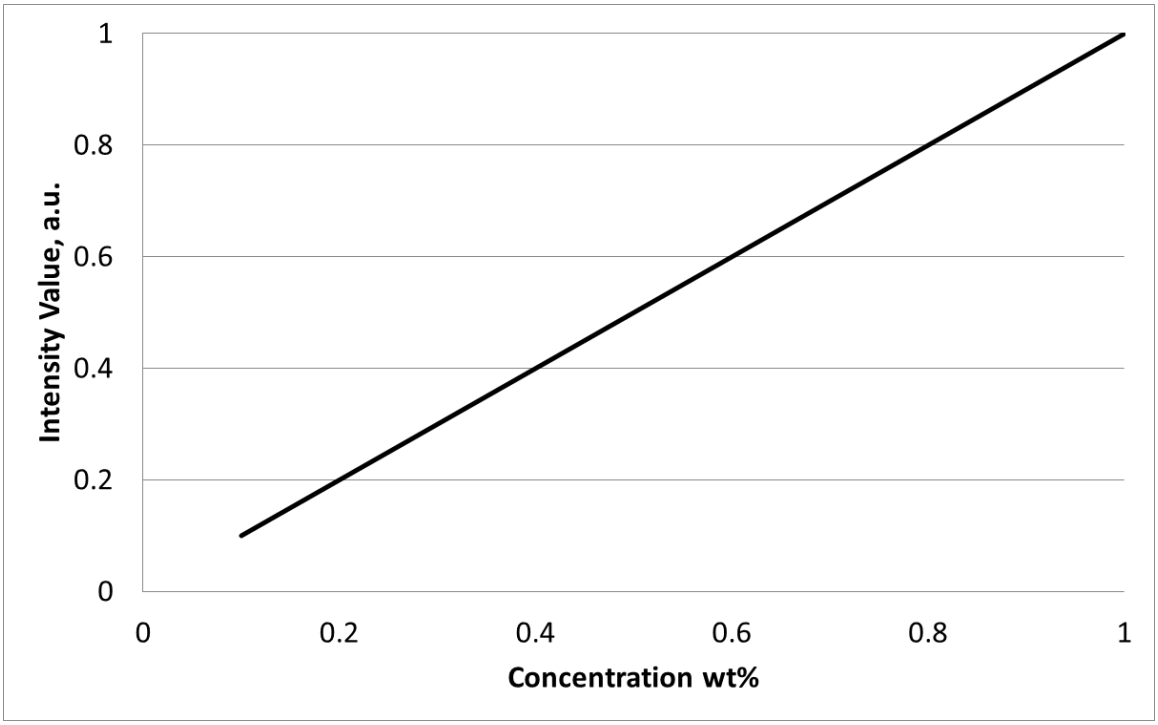

Figure 7. The diagram of the intensity variation of the scattered light with increase in the concentration

Also, the study has shown that there is a linear relationship between the refractive index and the concentration [73]. Equation 27 and Equation 29 provide a qualitative description of the intensity of the scattered light, when the refractive index or the concentration is changing.

4. EXPERIMENTAL METHODS

4.1 Sample Preparation

Gellan gum is an anionic microbial polysaccharide which is used as a gelling agent. Since it is water-soluble and has rapid phase transition (gelation) characteristics, it has been used in the food industry and biomaterial community. Gelzan^{TM} (Sigma Aldrich Chemical Co.) is a modified deacylated form of gellan and is the gellan used in all our hydrogel preparations. This modification gives the material transparency. To prepare the gels, gellan was dissolved at 2X the desired final concentration and heated to 60^{o}C in water. While at elevated temperature, the gellan was mixed 1:1 with 2X phosphate buffered saline (PBS) to introduce cations. Upon cooling in the presence of cations, gellan undergoes a temperature mediated random-coil to double helix formation. Additionally, the formed double helices can aggregate and form junction zones, resulting in a 3-D network held together by hydrogen bonding, forming a physical hydrogel. The refractive index of the hydrogel is approximately 1.33. Three different concentrations of gellan hydrogels were prepared. Also, six different sizes of nanobeads (polystyrene) were incorporated into the hydrogels. The refractive index of the nanobead is assumed to be similar to that of bulk polystyrene, which is listed for wavelengths of laser diode modules used. Table 3 shows the refractive index values with respect to the wavelength.

Table 3. The refractive index value of polystyrene with respect to the wavelength (refractive index values of polystyrene are acquired in refractiveindex.info)

	$405nm$	$520nm$	$532nm$	$635nm$	$780nm$
Refractive Index of the polymer	**1.6170**	**1.600**	**1.5983**	**1.5874**	**1.5790**

4.1.1 Polymer/Nanobead Hydrogels

Three different concentrations of ionic gellan hydrogels at 0.2, 0.3 and 0.4 wt% (Gelzan™, Sigma Aldrich Chemical Co.) were prepared. As the concentration of the gellan increases, the 3-D network will increase in density and the storage modulus increase exponentially. Also, six different sizes of nanobeads at 50, 100, 150, 200, 300 and 400 nm (Polysciences INC,) were incorporated into each concentration of hydrogel, giving a total of eighteen combinations. The speckle pattern images vary with respect to the size of the nanobead and density of the 3D-gel network. Table 4 shows the nominal sizes of the nanobead and the size ranges. Sodium azide (0.05%) was added in samples to prevent the growth of bacteria.

Table 4. Nominal size of nonobead and size range (the data is acquired from Polysciences, Inc.)

Nominal Size	Size Range
50nm	45.0-55.0nm
100nm	95.0-110.0nm
150nm	140.0-160.0nm
200nm	190.0-210.0nm
300nm	285.0-315.0nm
400nm	380.0-420.0nm

4.2 Slit-Lamp Modification

A conventional method to examine and diagnose eyes in ophthalmology and optometry areas is by using a slit lamp setup. This setup has been used for animal eye research both *in vitro* and *in vivo* due to its simplicity. The slit lamp setup uses white light as a light source for examining the eye.

The schematic of the modified slit lamp is shown in Figure 8. Three areas were modified: a) a illumination area, b) a beamsplitter tube area, and c) a video camera area. The slit lamp was modified in order to conduct future animal studies.

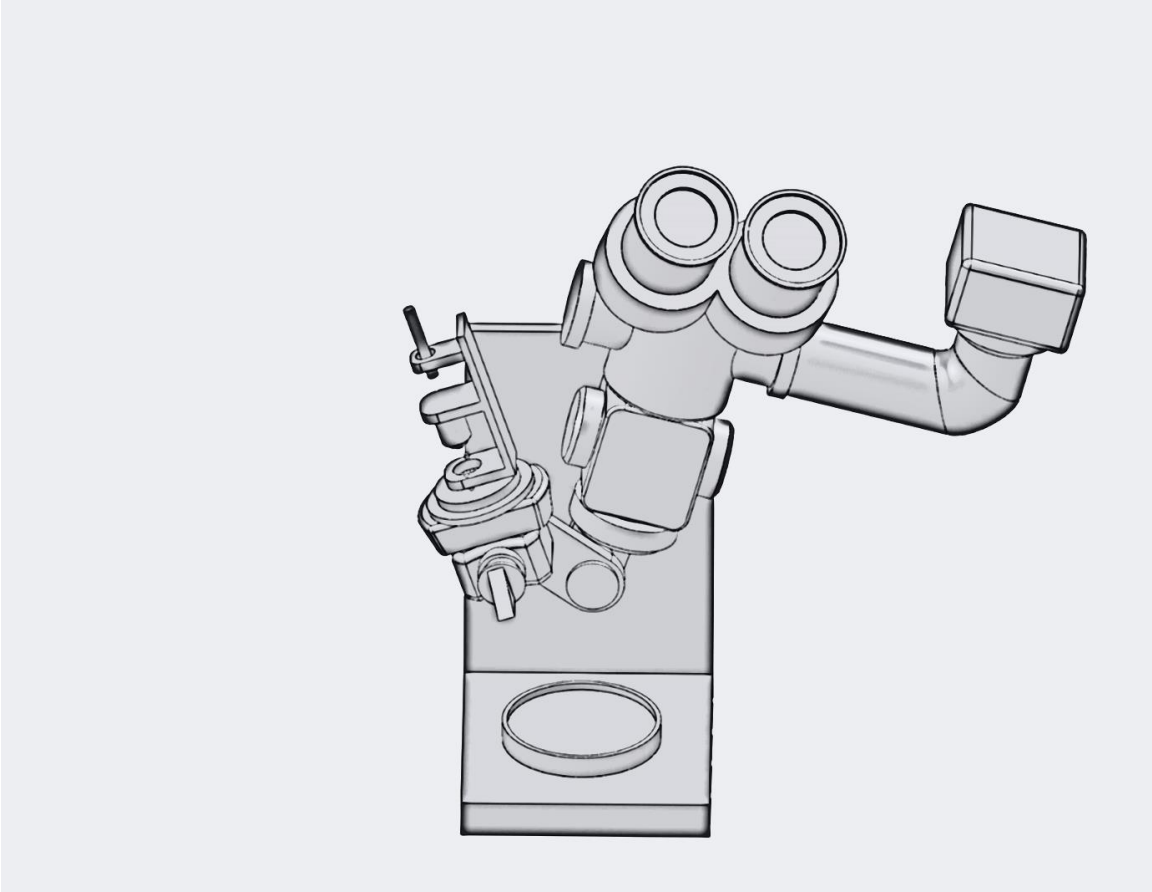

Figure 8. Schematic of the modified slit lamp setup (SolidWorks Software)

To modify this setup to study vitreous humor substitute, the white lamp assembly was removed and replaced with a custom fabricated laser diode mount and lens assembly. Figure 9 shows photographs of the illumination area. Figure 9a shows the disassembled illumination area, and Figure 9b shows that three customized brackets were mounted on the illumination area of the slit lamp to install the laser diode module along with a 40X

microscope objective to expand the laser beam. The laser diode module was used in the setup to increase the coherence length.

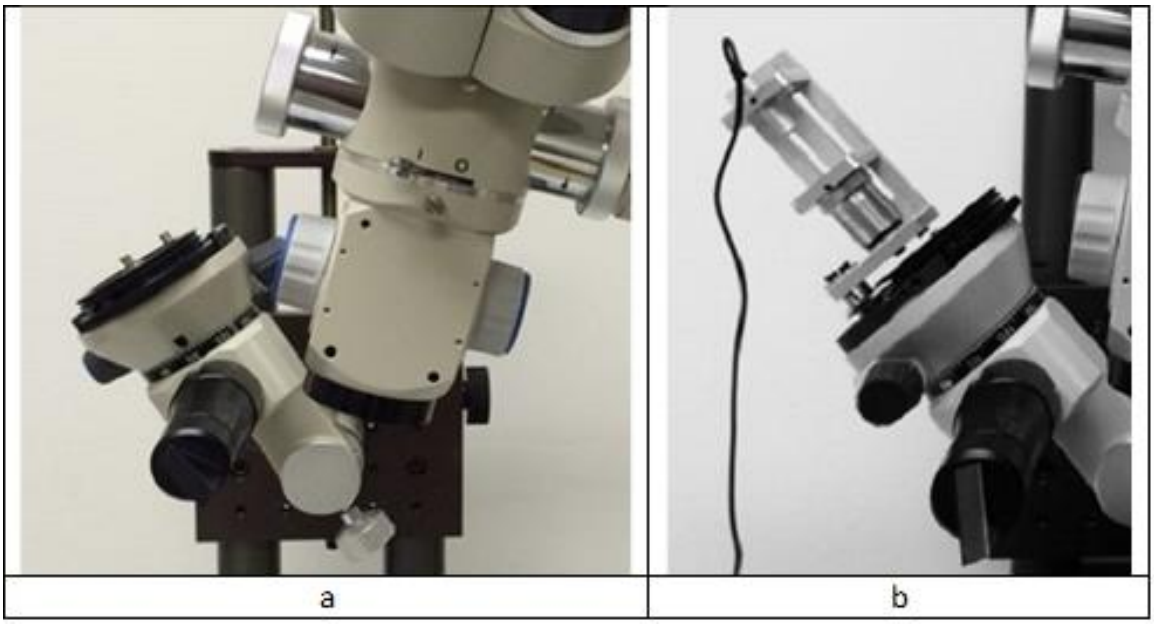

Figure 9. Photographs of the illumination area in the slit lamp. a) disassembled illumination area b) three customized brackets mounted on the illumination area of the slit lamp to install the laser diode module with a 40X microscope objective.

Figure 10 shows photographs of the beamsplitter tube area. An iris (SM1D25, Thorlabs) was mounted on the beamsplitter tube using a customized bracket.

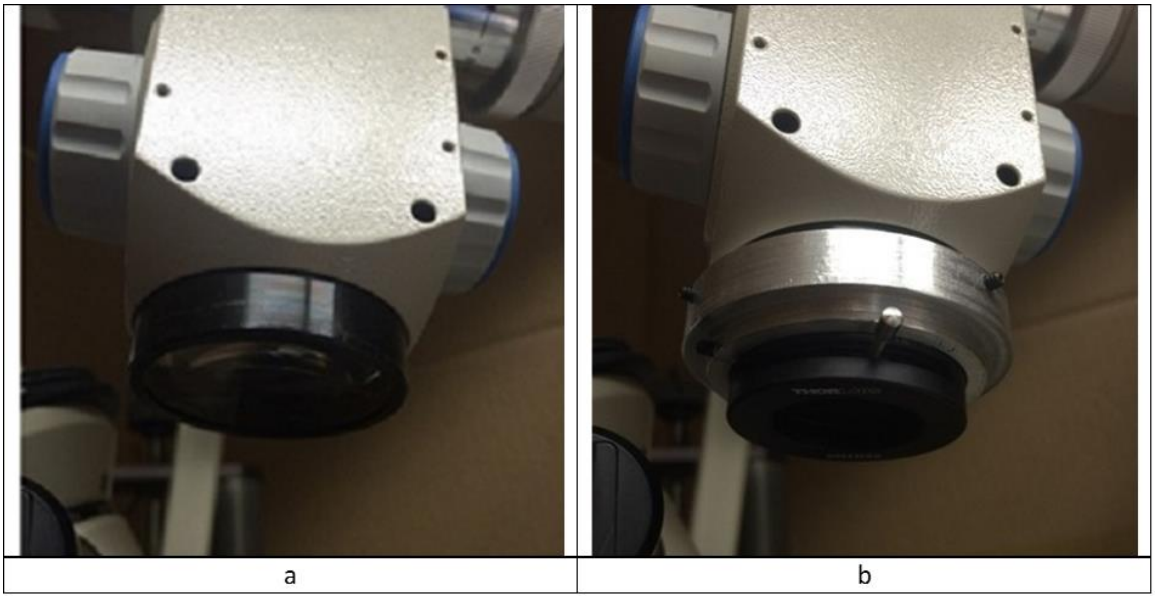

Figure 10. Photographs of the beamsplitter tube in the slit lamp a) before modification b) an iris, which controls the amount of the scattered light, and a custom fabricated bracket mounted on the beamsplitter tube.

Figure 11 shows photographs of the video camera adapter area. A CCD camera (DMK 21AU04 Monochrome Camera, The Imaging Source®) was mounted on the video camera adapter to record a speckle pattern image. The sensor (ICX098BL, Sony) of a CCD camera has 640×480 pixels, and each pixel size is 5.6 μm × 5.6 μm.

Figure 11. Photographs of the video camera area in the slit lamp. A CCD camera is mounted on the video camera adapter to record a speckle pattern image.

Figure 12 shows a photograph of the modified slit lamp. The modified slit lamp was mounted on an optical table (Oriel Instrument®) to isolate vibrations. A blackened background plate was attached to a z-translational stage, and the z-translational stage was mounted on the optical table. The setup was calibrated in order to find the plane of focus by changing the height of either the modified slit lamp or the z-translational stage. The prepared sample was located on top of the z-translational stage. The entire setup was covered using a cardboard frame with the inside layered with black fabric. The frame protected the camera from extraneous light.

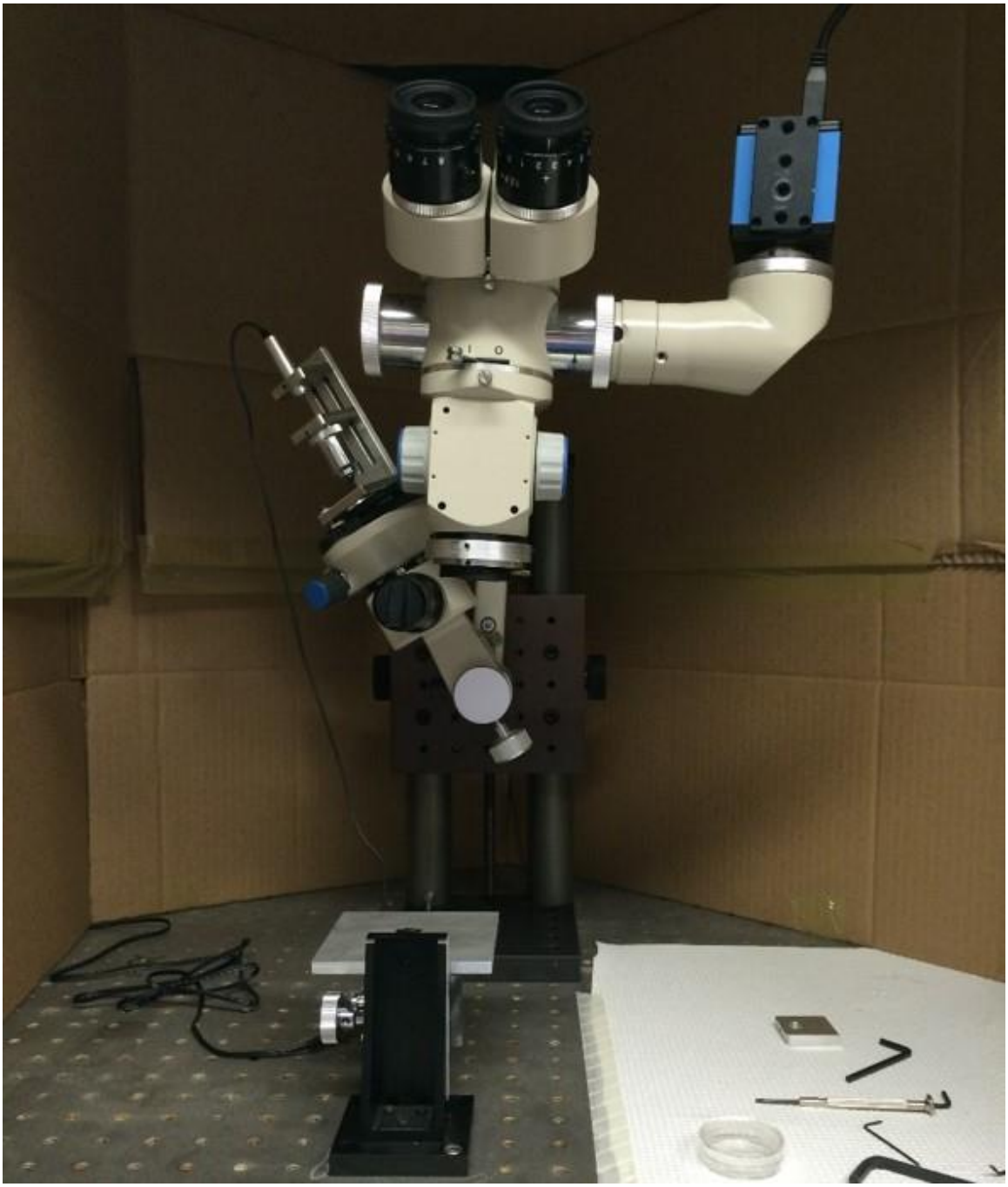

Figure 12. Photograph of the modified slit lamp setup.

4.3 Experimental Procedures

The schematic of the HWAM (Histogram Wavelength Analysis Method) apparatus is shown in Figure 13. The laser beam from a laser diode module was expanded by a lens and sent through a rectangular slit. Once the expanded beam passed through the rectangular slit, the shape of the expanded beam was changed to the rectangular shape. The width of the slit can be changed to control the size of the illuminating beam by using a rotating lever which is equipped on the slit tube.

The laser beam illuminated the biological specimen placed in a petri-dish which is on a blackened background plate. The blackened background plate was used to reduce unwanted speckle patterns formed from scattered light. The height of the specimen can be changed by the z-translational stage to allow the CCD to focus on different layers of the specimen so as to minimize the multiple scattering. The illuminating beam was set at an angle of θ_1, and a CCD camera was set at an angle of θ_2, each with respect to the surface normal. The speckle images were recorded by a CCD camera at constant angle for the experiment. The laser diode modules ((CPS405 ($\lambda = 405nm$), CPS520 ($\lambda = 520nm$), CPS532 ($\lambda = 532nm$), CPS635S ($\lambda = 635nm$), and CPS780S ($\lambda = 780nm$), Thorlabs)) were mounted in a custom fabricated mount that allowed for precise positioning of the lasers to create the same angle of illumination and the same divergence of the beam created by the beam expander (the microscope). This allowed the experiments to be performed under identical conditions with the different laser diodes. To

minimize the misalignment of the incident light, two fabricated brackets, representing different diameters of the laser diode modules, were utilized to arrange the laser diode modules in the same spot using set screws. Although the laser diode modules were nominally polarized along one axis, a small percentage of output power was unpolarized. The laser diode module consists of housing, laser diode, and collimating elements. Laser diode modules require a 5VDC power supply (LDS5, Thorlabs) to operate. Table 5 shows optical specifications of five laser diode modules.

Table 5. Optical specifications of five laser diode modules

	$405nm$	$520nm$	$532nm$	$635nm$	$780nm$
PER	22dB	25dB	4dB	22dB	25dB
% of Power	~99.3%	~99.7%	~71.5%	~99.3%	~99.7%
Beam Shape	Elliptical	Elliptical	Round	Elliptical	Elliptical
Power	4.5mW	4.5mW	4.5mW	4.5mW	4.5mW

In addition, the position of the petri-dish was also always located in the same spot as the vitreous humor substitute. Two images were recorded: one from the specimen and the petri-dish and the other from the petri-dish without any specimen. The two images were subtracted to eliminate the effect of the petri-dish. Digital images of the speckle pattern are in an 8-bit gray scale jpeg with a 640×480 pixel format and were imported to a PC. Each pixel's value varies from 0 to 255, and the speckle images are processed in a Matlab software environment (MathWorks®).

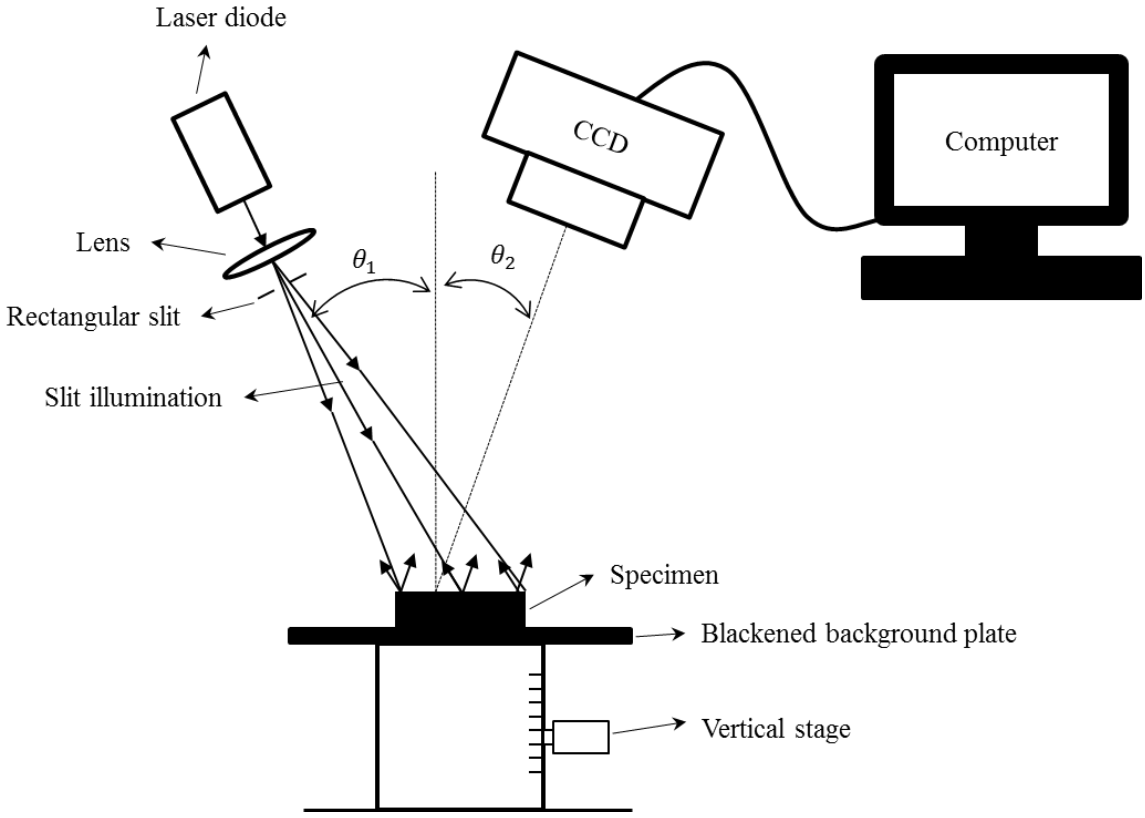

Figure 13. Schematic diagram of the experimental setup, where θ_1 and θ_2 are the incident and scattered angle respectively.

4.4 Data Analysis

In the experimental analysis, the histogram of the speckle pattern images are observed as a function of pixel numbers with respect to the intensity variations. Initially, the background speckle pattern with a blackened background plate and a petri-dish without a specimen is captured. Then, ten speckle patterns (10 FPS) are acquired in a sequence to overcome the constant fluctuating speckle pattern caused by the Brownian motion of the biological specimen. Recorded intensity speckle pattern images consist of 307,200 discrete pixels. The intensity values, $I(i,j)$, of each discrete pixel are expressed in grayscale ranging from 0 (black) to 255 (white). The spurious information, which might be coming from either the petri-dish or the blackened background plate, can be removed by using a simple subtraction method. To perform the subtraction process, the speckle pattern image from the empty-petri dish is subtracted from each speckle pattern image from the biological specimen, and same subtraction processes are repeated for the remainder of the speckle pattern images (10 subtraction process). All speckle patterns used in the experimental analysis have the background speckle pattern eliminated by such a process. The subtraction process is performed pixel by pixel. Only positive values are obtained, and negative values are set to zero. The subtraction operation is then processed in Matlab software. A diagram of the subtraction process is shown in Figure 14.

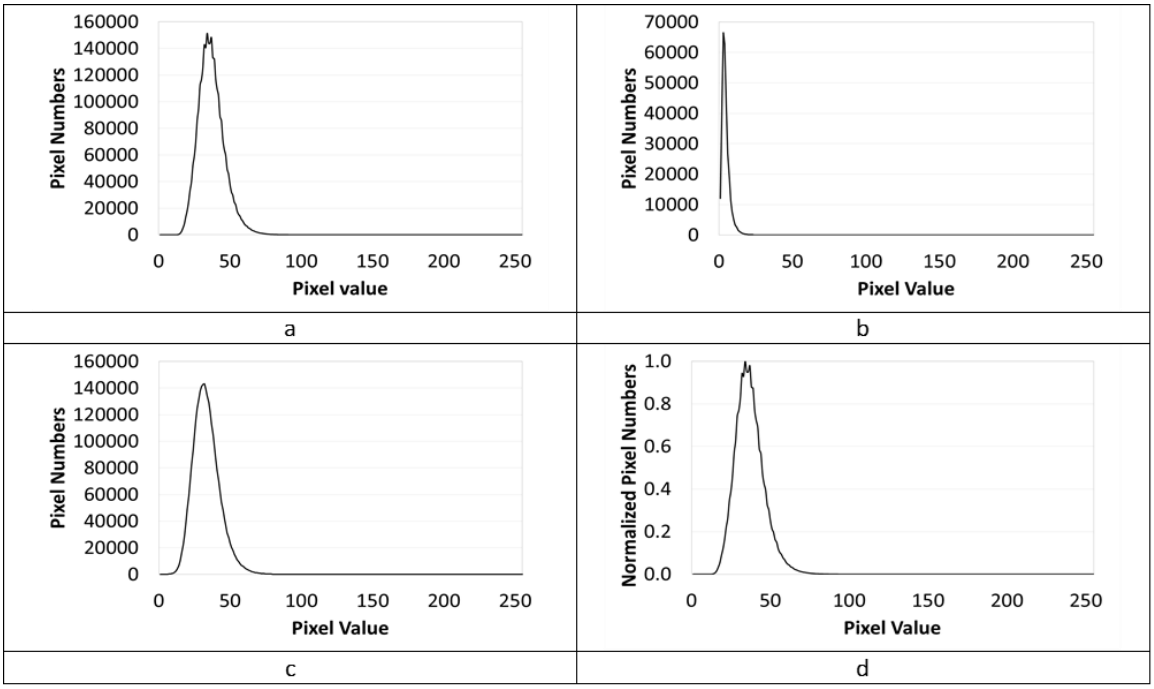

Figure 14. Diagram of the subtraction process using the intensity histogram in Matlab software. 'a' is the intensity histogram of the speckle pattern image from the biological specimen in the petri dish, 'b' is the intensity histogram of the speckle pattern image from the empty-petri dish, 'c' is the intensity histogram of the subtracted speckle pattern image, 'd' is the normalized intensity histogram of 'a'. (400 nm nanobead is embedded in 0.4 wt% biological specimen, the incident wavelength is 405 nm, and the scattering angle is 30°).

The intensity histogram of ten subtracted speckle pattern images is imported to Excel software, and the intensity values are distributed with respect to the pixel numbers

at each grayscale pixel value. Ten subtracted images are summed and averaged pixel by pixel at the identical pixel location with standard deviation values. Figure 15 illustrates the averaging process of the subtracted speckle pattern images.

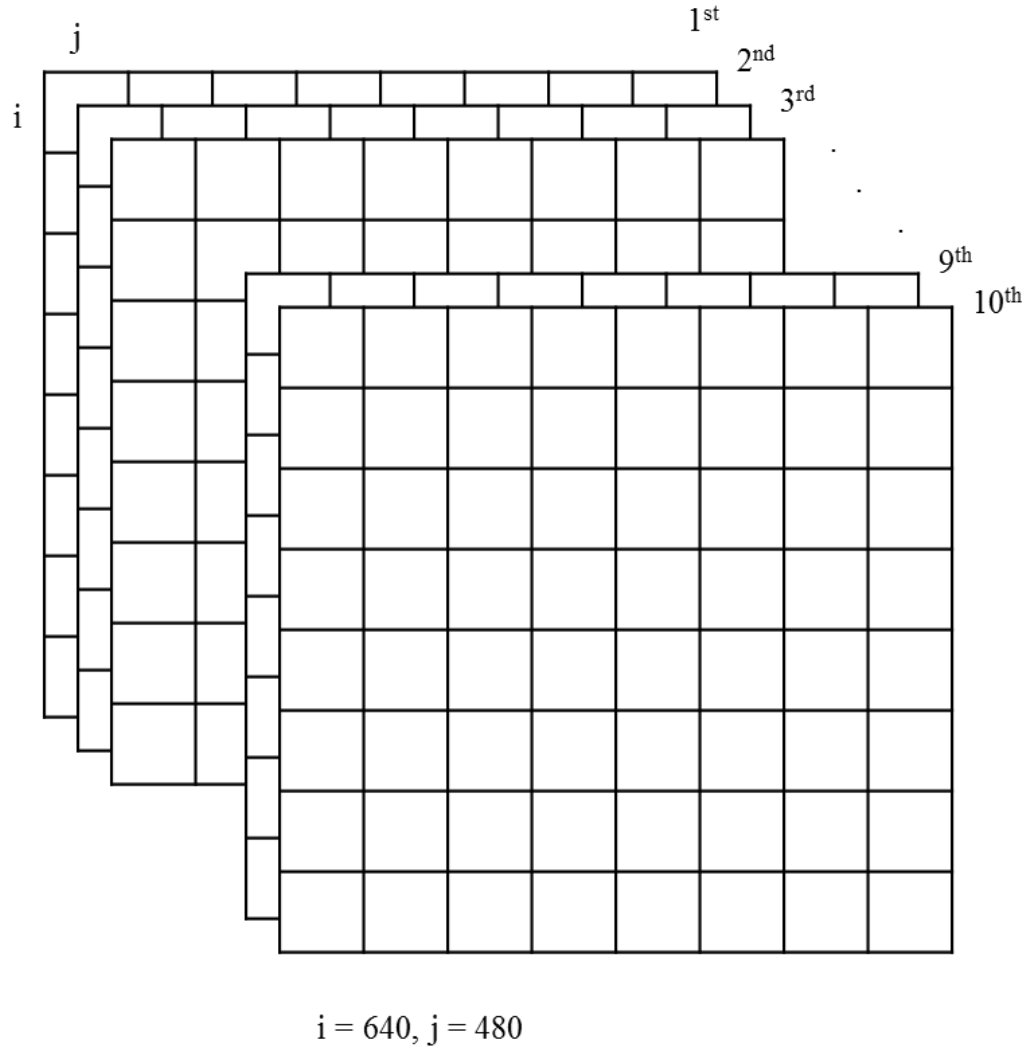

Figure 15. Schematic of the averaging process using the subtracted speckle pattern images in Excel software. 'i' stands for column and 'j' stands for row in the image.

The averaging of the speckle patterns reduces the effect of external turbulence caused by temperature and vibrations. The histogram of this final speckle pattern is generated from the analyzed speckle pattern. Each pixel is sorted in ascending order of the number of intensity values that occurred in the speckle pattern. In the analysis the intensity of the pixels is set such that it does not exceed the maximum value of the grey scale value of 255. For a given angle of illumination and observation, histogram plots as a function of the wavelength were obtained and the peak position values were extracted. Since the proposed theory shows that the scattering peak position is dependent on particle size, the size of the nanobeads in the vitreous humor substitute was held constant.

Six different specimens with increasing nanobead size are then used to obtain their histogram distribution. Figure 16 shows the normalized intensity histograms from the speckle images for one specific angle of illumination as the nanobead size is changed.

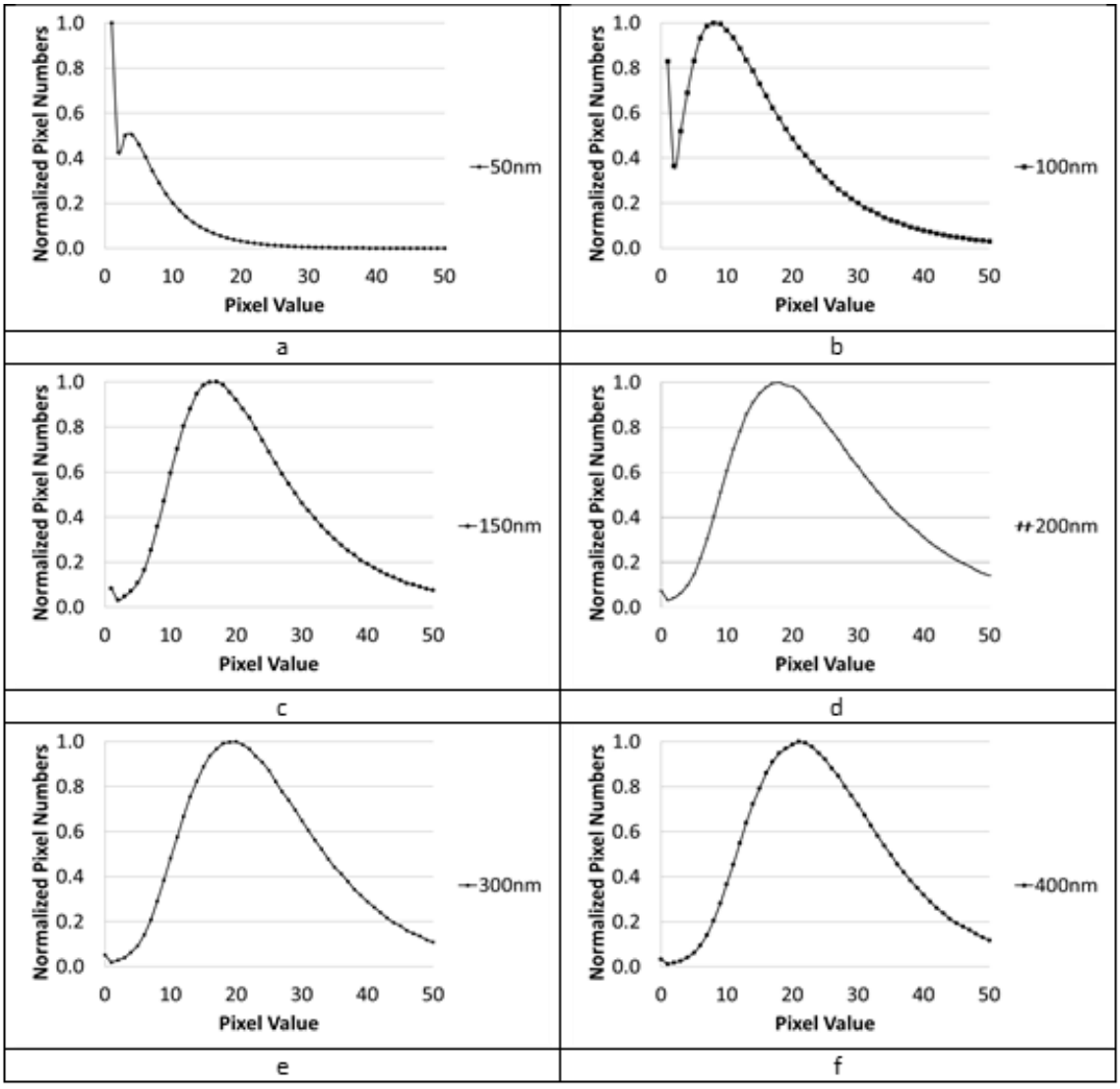

Figure 16. Diagrams of the normalized intensity histogram. a) 50 nm, b) 100 nm, c) 150 nm, d) 200 nm, e) 300 nm, f) 400 nm nanobead size (0.4 wt% biological specimen, the incident wavelength is 520 nm, and the scattering angle is 30°)

In Figure 17, the plots from Figure 16a-f were combined in order to better compare the results.

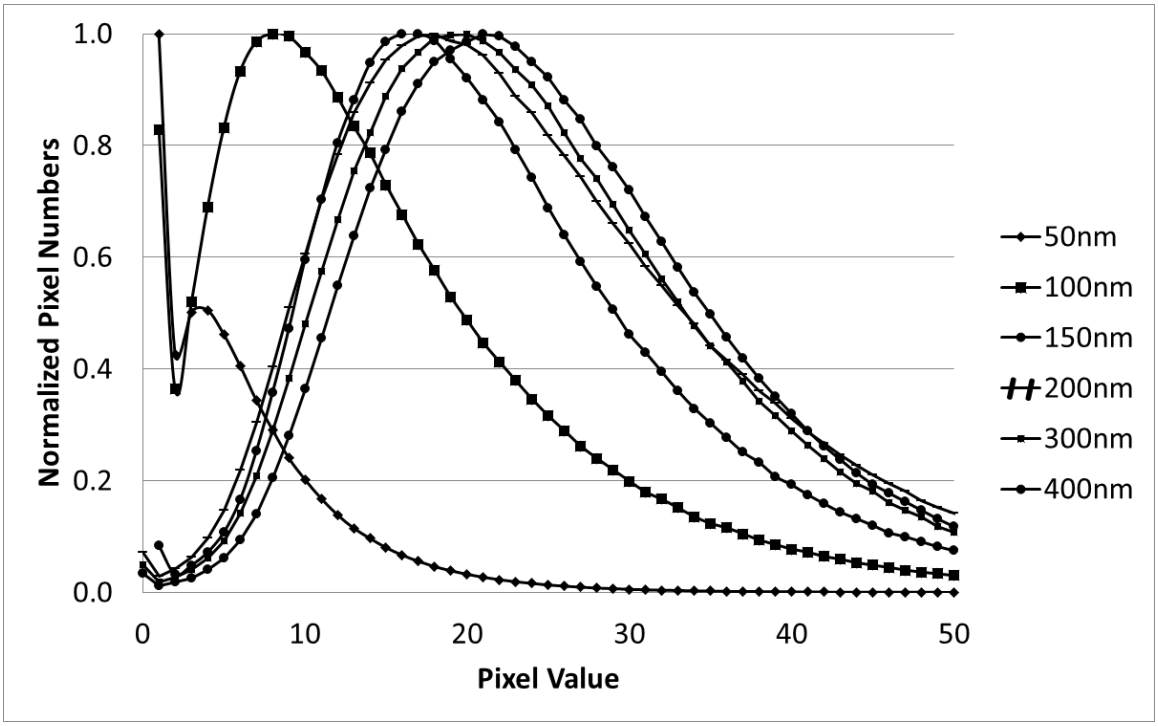

Figure 17. Diagram of the normalized intensity histogram with six different nanobead sizes (0.4 wt% biological specimen, the incident wavelength is 520 nm and scattering angle is 30°).

Figure 18 shows the normalized intensity histograms from the speckle images for one specific angle of illumination of 30° and with a nanobead size of 400 nm as the wavelength of the light is changed.

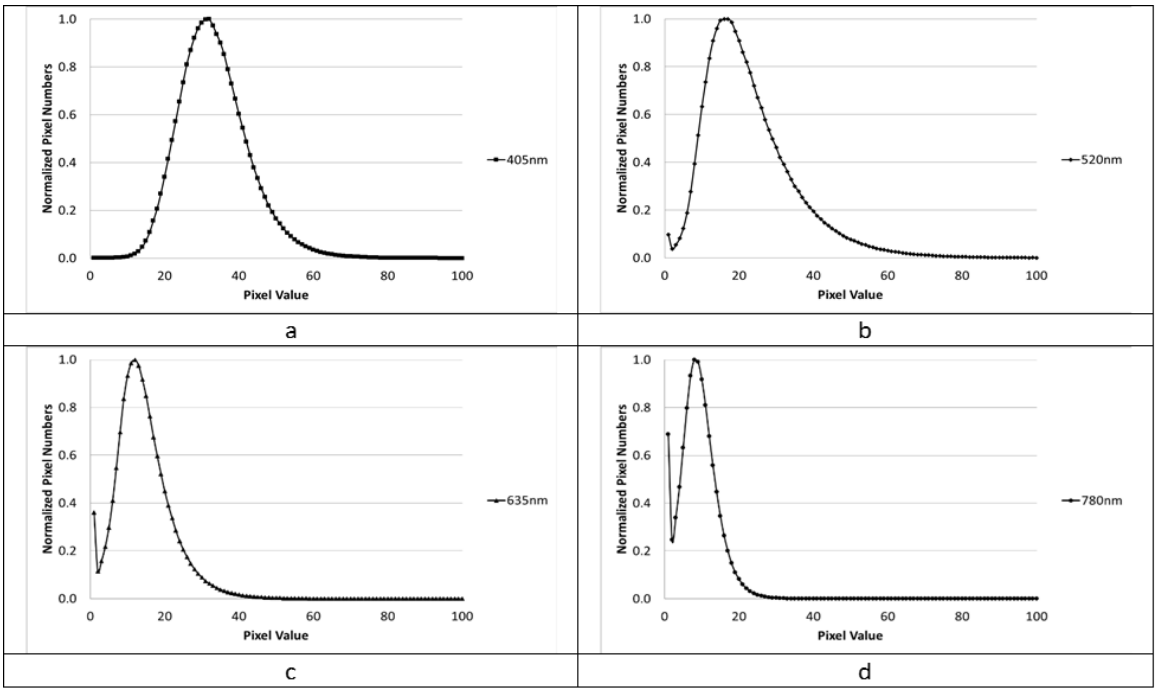

Figure 18. Diagrams of the normalized intensity histogram. a) λ=405 nm, b) λ=520 nm, c) λ= 635 nm, and d) λ=780 nm with 400 nm nanobeads embedded in 0.4 wt% biological specimen and scattering angle is 30°.

The intensity histograms from the speckle images for one specific angle and nanobead size are incorporated in one histogram for comparison and the histogram is shown in Figure 19.

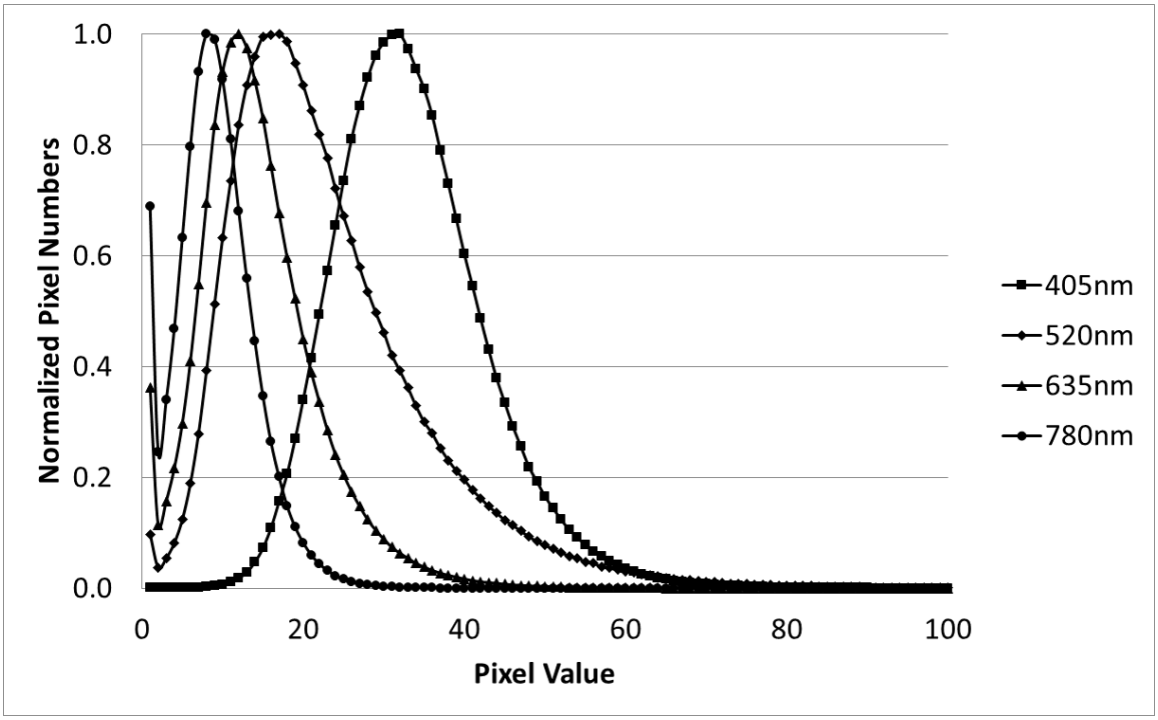

Figure 19. Diagram of the normalized intensity histogram with four different wavelengths (400 nm nanobead is embedded in a 0.4 wt% biological specimen and a scattering angle of 30°)

5. EXPERIMENTAL RESULTS

For the histogram plots created from the average 10 speckle images, a peak point appeared in the histogram. The location of the peak point varied with respect to nanobead size and wavelength of the incident light. The collected peak point data can be incorporated in one diagram, which shows a peak shift point. The shift in the peak (i.e peak shift value) was calculated with respect to the origin for each nanobead size. Figure 20 shows the shift as a function of wavelength for nanobead sizes of 50 nm, 100 nm, 150 nm, 200 nm, 300 nm, and 400 nm. As the wavelength of the incident beam increases, the amount of peak shift decreases. Also, the decay rate is found to be slow when the nanobead size is increased. Figure 20 shows the peak shift with respect to the nanobeads size and the wavelengths.

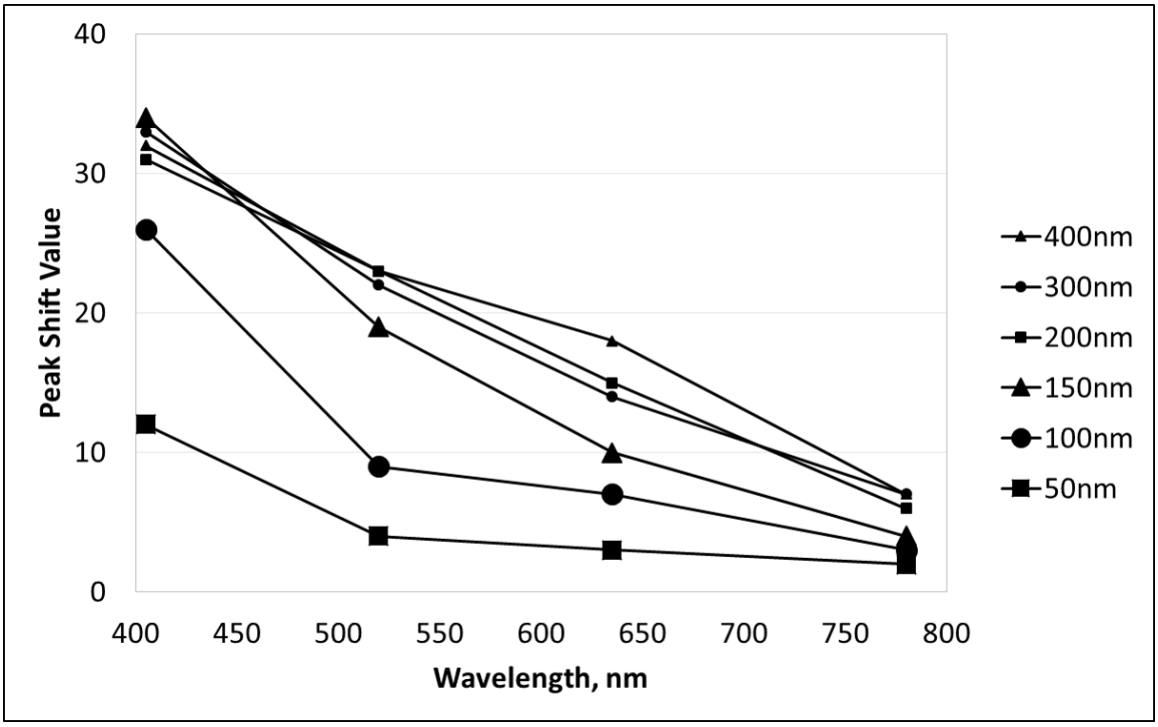

Figure 20. Diagram of the peak shift with respect to the nanobead sizes and the wavelengths (0.4 wt% biological specimen and scattering angle of 30°)

Table 6 shows standard deviation values of the peak shift value from the averaged speckle pattern image. The standard deviation values belong to Figure 20.

Table 6. Standard deviation values of the peak shift value from the averaged speckle pattern image with respect to the wavelength of light and the size of a nanobead (0.4 wt% biological specimen and scattering angle of 30°)

	$50nm$	$100nm$	$150nm$	$200nm$	$300nm$	$400nm$
$405nm$	0.16754	0.22563	0.22576	0.24072	0.24732	0.24524
$520nm$	0.10104	0.22045	0.22035	0.23268	0.23754	0.23467
$635nm$	0.08190	0.19082	0.20813	0.24086	0.23961	0.24404
$780nm$	0.06966	0.08361	0.09955	0.14893	0.18051	0.16303

The peak shift point of the experimental results is normalized to compare the experimental results with the theoretical values. Figure 21 shows the normalized peak point shift with respect to the nanobead size and the wavelength of the light. It can be seen from the plot that the decay rates overlaps for particle size greater than 200 nm. However, it is possible to discern the decay rate for particle size less than 200 nm.

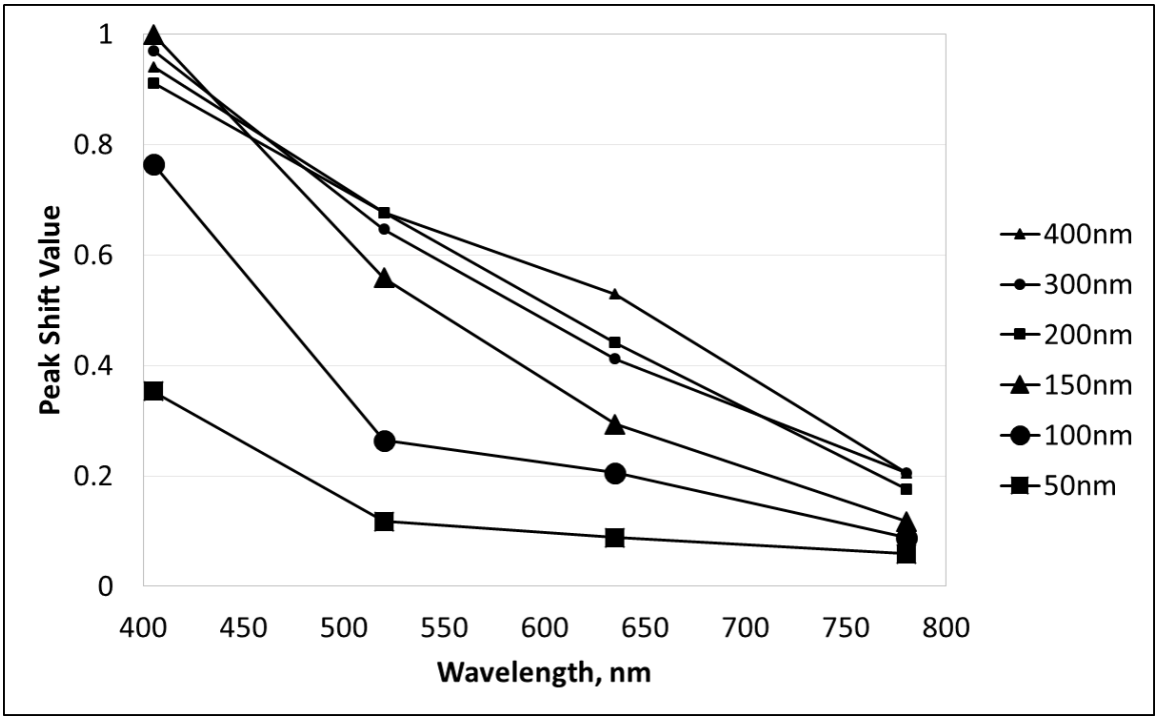

Figure 21. Diagram of the normalized peak shift with respect to the nanobead size and the wavelengths (0.4 wt% biological specimen and scattering angle of 30°)

To compare the normalized peak point shift values to the theoretical peak point shift value, the peak shift value of each particle size plot is scaled to be 1, and the rest of the values for the given nanobead are also scaled by the same ratio which is shown in Figure 22.

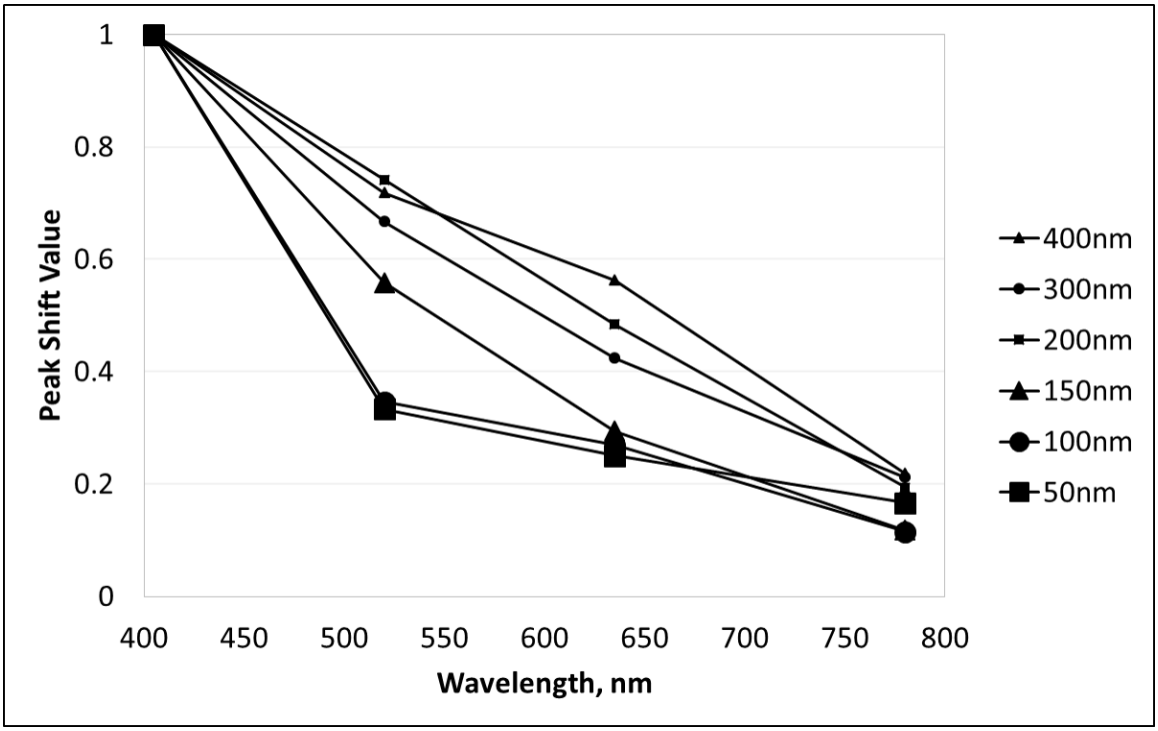

Figure 22. Diagram of the normalized peak shift where the peak shift values are set to be 1 (the wavelength used is 405 nm, the specimen is 0.4 wt% biological specimen and scattering angle of 30°)

Figure 23 shows the theoretical peak point shift and the normalized experimental peak point shift with respect to the nanobead size and the wavelength of the light. Figure 23a shows the plot for 50 nm nanobead size in the vitreous humor substitute. The theoretical results indicate the degree to which the experimental results follows Rayleigh scattering or Mie scattering. The data matches our proposed theory very closely when c_1

is 0.9 and c_2 is 0.1. Figure 23b and Figure 23c show the plots for 100 nm and 150 nm nanobeads in the vitreous humor substitute respectively. The experimental results for 100 nm and 150 nm correspond our theory when c_1 is 0.9 and c_2 is 0.1. The results show that for 50, 100, and 150 nm nanobead particle size, the dominant scattering is Rayleigh. Figure 23d shows the plot for 200 nm nanobeads in the vitreous humor substitute, and the experimental result matches our proposed theory when c_1 is 0.6 and c_2 is 0.4. This result indicates that for 200 nm nanobead particle size, the dominant scattering is Rayleigh. Figure 23e shows the plot for 300 nm nanobeads in the vitreous humor substitute, and the experimental result matches our proposed theory when c_1 is 0.4 and c_2 is 0.6. Figure 23f shows the plot for 400 nm nanobeads in the vitreous humor substitute, and the experimental result matches our proposed theory when c_1 is 0.3 and c_2 is 0.7. The results indicate that for 300, and 400 nm nanobead particle size, the dominant scattering is Mie.

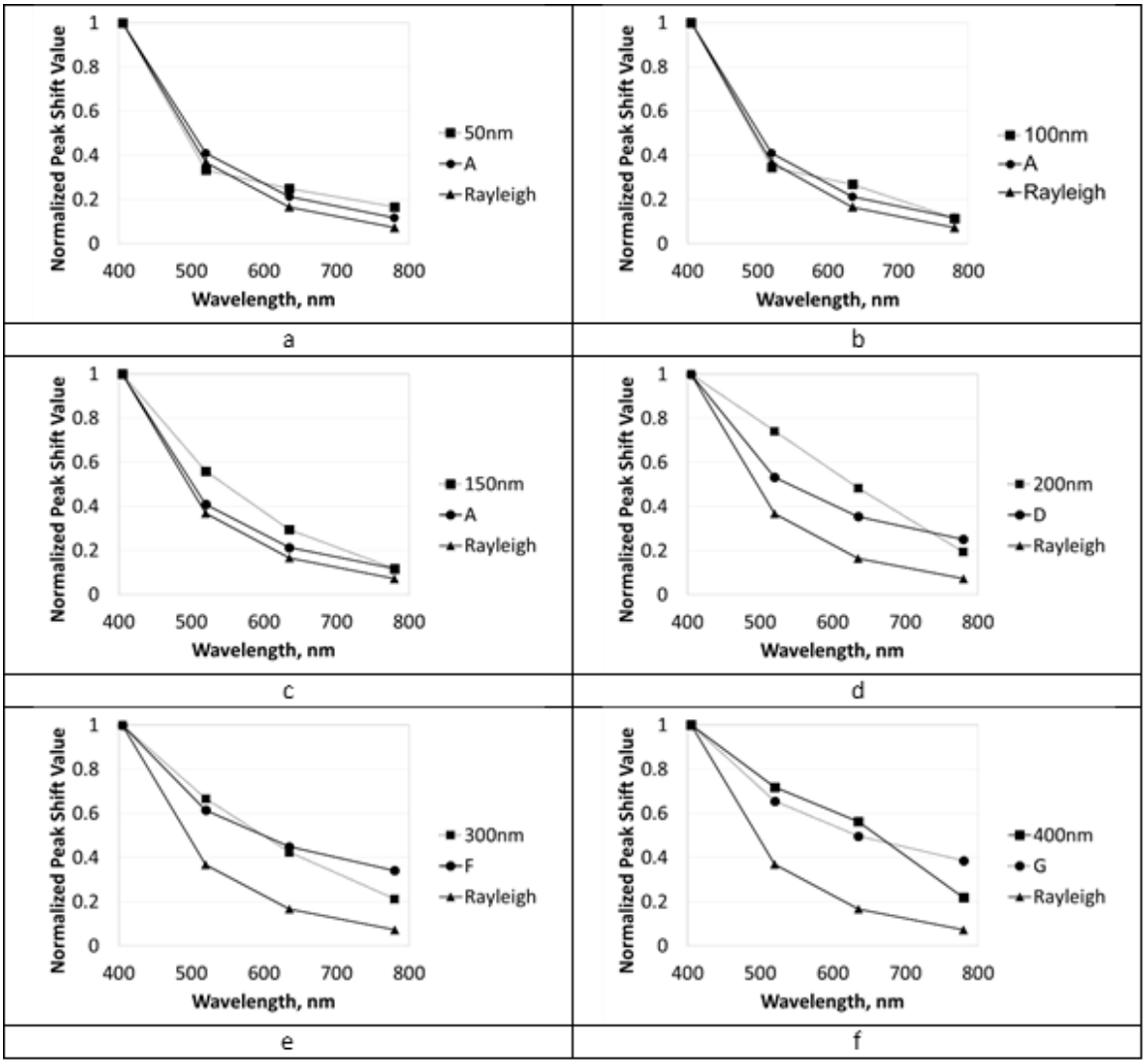

Figure 23. Diagram of the normalized peak shift and the theoretical peak shift with respect to the nanobead size and the wavelength of the light used a) 50 nm, b) 100 nm, c) 150 nm, d) 200 nm, e) 300 nm, and f) 400 nm (0.4 wt% biological specimen and scattering angle of 30°).

6. CONCLUSIONS

Over the past decade, speckle related phenomena have been studied by researchers because this method is simple yet produces reliable results. The scattering property of a sample modeling vitreous humor using the histogram of the speckle pattern formed due to back scattering of light was studied in this thesis. The peak value displayed in the histogram was found to shift as the wavelength of light was changed, and this shift was found to have direct relationship to the particle size of the nanobeads in the specimen. The Histogram Wavelength Analysis Method (HWAM) is presented in the thesis to study biological material. The results show that there is a correlation between the intensity distribution of speckle pattern images, the wavelength of light, and nanobead size. In this technique, the shift in the peak of the histogram is extracted. For nanobead size less than 200 nm, the plots follow Rayleigh scattering theory. For nanobead sizes above 200 nm, the plots follow the proposed modified Rayleigh scattering theory pretty well along with Mie scattering. This noncontact method can be used to study vitreous humor and can be used to determine the size of the molecules when less than 200 nm in size.

7. FUTURE WORK

This work has shown that HWAM can be used to identify nanobead size less than 200 nm. In future studies, HWAM should be further investigated in order to see if it can be used to study the concentration dependency of a biological sample and the dependency on the angle of illumination.

Further, Fourier Transform algorithms and filtering algorithms can be employed to analyze the speckle pattern. Fourier Transform algorithms will convert the domain from space to spatial frequency so two or more different frequencies are used so that vitreous humor substitute can contain different sized molecules and nanobeads. Filtering algorithms can then be used to isolate the frequency from the analyzed data.

LIST OF REFERENCES

[1] J. W. Goodman, "Some fundamental properties of speckle," *Optical Society of America,* vol. 66, no. 11, pp. 1145-1150, November 1976.

[2] A. Zdunek, A. Adamiak, P. M. Pieczywek and A. Kurenda, "The biospeckle method for the investigation of agricultural crops:A review," *Optical and Lasers in Engineering,* vol. 52, pp. 276-285, 2014.

[3] J. D. Briers, "Laser speckle contrast imaging for measuring blood flow," *Optica Applicata,* vol. XXXVII, no. 1-2, pp. 139-152, 2007.

[4] R. P. Godinbo, M. M Silva, J. R. Nozela and R. A Braga, "Online biospeckle assessment without loss of definition and resolution by motion history image," *Optics and Lasers in Engineering,* vol. 50, pp. 366-372, 2012.

[5] R. Arizaga, M. Trivi and H. Rabal, "Speckle time evolution characterization by the co-occurrence matrix analysis," *Optics & Laser Technology,* vol. 31, pp. 163-169, 1999.

[6] M. Z. Ansari and A. K. Nirala, "Assessment of bio-activity using the methods of inertia moment and absolute value of the difference," *Optic,* vol. 124, pp. 512-516, 2013.

[7] H. Fujii, K. Nohira, Y. Yamamoto, H. Ikawa and T. Ohura, "Evaluation of blood flow by laser speckle image sensing. Part 1," *Applied Optics,* vol. 26, no. 24, pp. 5321-5325, 1987.

[8] P. D. Minz and A. K. Nirala, "Bio-activity assessment of fruits using generalized difference and parameterized Fujii method," *Optik,* vol. 125, pp. 314-317, 2014.

[9] R. A. Braga, C. M. B. Costa, T. Safade and F. M. D. costa, "Evaluation of activity through ynamic laser speckle using the absolute value of the differences," *Optics Communication,* vol. 284, pp. 646-650, 2011.

[10] C. Dainty and M. Chen, "Reflections on Speckle: Old and New Results," in *SPIE proceeding*, 2011.

[11] F. Fankhauser, Lasers in Ophthalmology: Basic, Diagnostic and Surgical Aspects; a Review, Kugler Publications, 2003.

[12] J. W. Goodman, Speckle Phenomena in Optics:Theory and Applications, Roberts and Company Publishers, 2007.

[13] D. A. Boas and A. K. Dunn, "Laser speckle contrast imaging in biomedical optics," *Biomedical Optics,* vol. 15, no. 1, pp. 1-12, 2010.

[14] J. D. Briers, "Laser Doppler, speckle and related techniques for blood perfusion mapping and imaging," *Physiological Measurement,* vol. 22, pp. R35-R66, 2001.

[15] G. H. Kaufmann, Advances in Speckle Metrology and Related Techniques, John Wiley & Sons, 2011.

[16] J. W. Goodman, "Statistical properties of laser speckle patterns," in *Laser Speckle and Related phenomena in series Topics in Applied Physics*, vol. 9, Springer-Verlag, 1984.

[17] J. C. Dainty, "The Statistics of speckle patterns," *Progress in Optics,* vol. 14, pp. 1-46, 1976.

[18] J. D. Briers, "Laser speckl techniques in biology and medicine," in *SPIE proceedings*, 1994.

[19] O. Carvalho, B. Clairac, M. Benderitter and L. Roy, "Statistical speckle study to characterize scattering media: use of two complementary approaches," *Optics Express,* vol. 15, no. 21, pp. 13817-13831, 2007.

[20] M. Draijer, E. Hondebrink, T. V. Leeuwen, W. Steenbergen, "Review of laser speckle contrast techniques for visualizing tissue perfusion," *Laser in Medical Science*, vol. 24, pp. 639-651, 2009.

[21] D. Briers, D. D. Duncan, E. Hirst, S. J. Kirkpatrick, M. Larsson, W. Steenbergen, W. Stromberg and O. B. Thompson, "Laser speckle contrast imaging: theoretical and practical limitations," *Biomedical Optics,* vol. 18, no. 6, 2013.

[22] M. J. Draijer, E. Hondebrink, M. Larsson, T. G. V. Leeuwen and W. Steenbergen, "Relation between the contrast in time integrated dynamic speckle patterns and the power spectral density of their temporal intensity fluctuations," *Optics Express,* vol. 18, no. 21, pp. 21883-21891, 2010.

[23] A. Humeau-Heurier, G. Mahe and P. Abraham, "Microvascular blood flow monitoring with laser speckle contrast imaging using the generalized differences algorithm," *Microvascular Research,* vol. 98, pp. 54-61, 2015.

[24] H. C. v. d. Hulst, Light scattering by Small Particles, Courier Corporation, 1957.

[25] R. Pecora, Dynamic Light Scattering: Applications of Photon Correlation Spectroscopy, Springer Science & Business Media.

[26] B. J. Berne and R. Pecora, Dynamic Light Scattering: with Applications to Chemistry, Biology, and Physics, Courier Corporation, 2000.

[27] D. A. Boas, C. Pitris and N. Ramanujam, Handbook of Biomedical Optics, CRC Press, 2011.

[28] L. V. Wang and H. Wu, Biomedical Optics:Principles and Imaging, Wiley, 2007.

[29] R. R. Zare, Laser Experiments for Beginners, University Science Books, 1995.

[30] K. Muraoka and M. Maeda, Lasdr-Aided Diagnostics of Plasmas and Gases, CRC Press.

[31] A. M. Pozo, J. J. Castro, and M. Rubino, "Optical characterization of display screens by speckle patterns," *Optical Engineering*, vol. 52, no. 10, 2013.

[32] D. Corradini, E. Eksteen (Katz), R. Eksteen, P. Schoenmakers, and N. Miller, Handbook of HPLC, CRC Press, 2011.

[33] H. Elim, B. Cai, O. Sugihara, T. Kaino, and T. Adschiri, "Size and concentration-dependent of Rayleigh scattering properties of titanium dioxide nanohybrid polymer," in *SPIE Proceedings*, 2010.

[34] W. Mahmood bin Mat Yunus, and Azizan bin Abdul Rahman, "Refractive index of solutions at high concentrations," *Applied Optics*, vol. 27, no. 16, 19883341-3343.

[35] H. J. Rabal and R. A. Braga Jr, Dynamic laser speckle and applications, CRC Press, 2008.

[36] Z. Xu, C. Joenathan and B. M. Khorana, "Temporal and spatial properties of the time-varying speckles of botanical specimens," *Optical Engineering*, vol. 34, no. 5, pp. 1487-1502, 1995.

[37] A. Mazhar, D. J. Cuccia, T. B. Rice, S. A. Carp, A. J. Durkin, D. A. Boas, B. Choi and B. J. Tromberg, "Laser speckle imaging in the spetial frequency domain," *Biomedical Optics Express*, vol. 2, no. 6, pp. 1553-1563, 2011.

[38] T. Xu, H. Hozan and G. R. Bashford, "In vivo lateral blood flow velocity measurement using speckle size estimation," *Ultrasound in Medicine & Biology,* vol. 40, no. 5, pp. 931-937, 2014.

[39] H. J. Rabal, N. Cap, M. Trivi and M. N. Guzman, "Q-statics in dynamic speckle pattern analysis," *Optics and Lasers in Engineering,* vol. 50, pp. 855-861, 2012.

[40] I. Passoni, A. D. Pra, H. Rabal, M. Trivi and R. Arizaga, "Dynamic speckle processing using wavelets based entropy," *Optics Communications,* vol. 246, pp. 219-228, 2005.

[41] R. S. Sirohi, Speckle Metrology, CRC Press, 1993.

[42] J. M. Burch, "Laser speckle metrology," in *SPIE Proceedings*, 1971.

[43] A. W. Lohmann and G. P. Weigelt, "Speckle methods for the display of motion paths," *Optical Society and America,* vol. 66, no. 11, pp. 1271-1274, 1976.

[44] S. A. El-said and A. T. Azar, "Speckles suppression techniques for ultrasound images," *Medical Imaging and Radiation Sciences,* vol. 43, no. 4, pp. 200-213, 2012.

[45] A, Achim, A. Bezerianos and P. Tsakalides, "Novel Bayesian multiscale method for speckle removal in medical ultrasound images," *Transactions on Medical Imaging,* vol. 20, no. 8, pp. 772-783, 2001.

[46] M. Karaman, M. A. Kutay and G. Bozdagi, "An adaptive speckle suppression filter for medical ultrasonic imaging," *Transactions on Medical Imaging,* vol. 14, no. 2, pp. 283-292, 1995.

[47] T. Loupas, W. N. McDicken and P. L. Allan, "An adaptive weighted median filter for speckle suppression in medical ultrasonic images," *Circuits and Systems*, vol. 36, no. 1, pp. 129-135, 1989.

[48] J. Lee, "Speckle suppression and analysis for synthetic aperture radar images," *Optical Engineering,* vol. 25, no. 5, pp. 636-643, 1986.

[49] A. A. Mudassar and S. Butt, "Improved digital image correlation for in-plane displacement measurement," *Applied Optics,* vol. 53, no. 5, pp. 960-970, 2014.

[50] I. Yamaguchi and K. Kobayshi, "Speckle displacement in holographic and speckle metrology," in *SPIE Proceedings*, 2011.

[51] B. Pan, K. Qian, H. Xie and A. Asundi, "Two-dimensional digital image correlation for in-plane displacement and strain measurement:a review," *Measurement Science and Technology*, 2009.

[52] R. M. Groves, S. Fu, S. W James and R. P Tatam, "Single-axis combined shearography and digital speckle photography instrument for full surface strain characterization," *Optical Engineering*, vol. 44, no. 2, 2005.

[53] J. C. Ramirez-San-Juan, C. Regan, B. Coyotl-Ocelotl and B. Choi, "Spatial versus temporal laser speckle contrast analyses in the presence of static optical scatterers," *Biomedical Optics*, vol. 19, no. 10, 2014.

[54] C. P. Valdes, H. M. Varma, A. K. Kristoffersen, T. Dragojevic, J. P. Culver and T. Durduran, "Speckle contrast optical spectroscopy, a non-invasive, diffuse optical method for measuring microvascular blood flow in tissue," *Biomedical Optics Express*, vol. 5, no. 8, pp. 2769-2784, 2014.

[55] J. C. Ramirez-San-Juan, E. Mendez- Aguilar, N. Salazar-Hermenegildo, A. Fuentes-Garcia, R. Ramos-Garcia and B. Choi, "Effects of speckle/pixel size ratio on temporal and spatial speckle-contrast analysis of dynamic scattering systems: Implications for measurements of blood-flow dynamic," *Biomedical Optic Express*, vol. 4, no. 10, pp. 1883-1889, 2013.

[56] A. K. Dunn, "Laser speckle contrast imaging of cerebral blood flow," *Annals of Biomedical Engineering*, vol. 40, no. 2, pp. 367-377, 2013.

[57] O. Thompson, M. Andrews and E. Hirst, "Correction for spatial averaging in laser speckle contrast analysis," *Biomedical Optic Express*, vol. 2, no. 4, pp. 1021-1029, 2011.

[58] T. M. Le, J. S. Paul, H. Al-Nashash, A. Tan, A. R. Luft, F. S. Sheu and S. H. Ong, "New insights into image processing of cortical blood flow monitors using laser

speckle imaging," *Transactions on Medical Imaging,* vol. 26, no. 6, pp. 833-842, 2007.

[59] J. D. Briers and S. Webster, "Laser speckle contrast analysis(LASCA): A nonscanning, full-field technique for monitoring capillary blood flow," *Biomedical Optics,* vol. 1, no. 2, pp. 174-179, 1996.

[60] O. Carvalho, S. Guyot, L. Roy, M. Benderitter and B. Clairac, "Speckle: tool for diagnosis assistance," in *SPIE Proceedings*, 2006.

[61] Y. Piederriere, F. Boulvert, J. Cariou, B. L. Jeune, Y. Guern and G. L. Brun, "Backscattered speckle size as a function of polarization: influence of particle-size and -concentration," *Optics Express,* vol. 13, no. 13, pp. 5030-5039, 2005.

[62] S. Guyot, M.Peron and E. Delechelle, "Spatial speckle characterization by Brownian motion analysis," *Physical Review,* p. 046618, 2004.

[63] Y. Aizu and T. Asakura, "Bio-speckle phenomena and their application to the evaluation of blood flow," *Optics & Laser Technology,* vol. 23, no. 4, pp. 205-219, 1991.

[64] M. Ogami, R. Kulkarni, H, Wang, R. Reif and R. K. Wang, "Laser speckle contrast imaging of skin blood perfusion responses induced by laser coagulation," *Quantum Electronics,* vol. 44, no. 8, pp. 746-750, 2014.

[65] A. F. Fercher and J. D. Briers, "Flow visualization by means of single-exposure speckle photography," *Optics Communications,* vol. 37, no. 5, pp. 326-330, 1981.

[66] E. Klijn, H. C. Hulscher, R. K. Balvers, W. P. Hollland, J. Bakker, A. J. Vincent, C. M. Dirven and C. Ince, "Laser speckle imaging identification of increases in cortical microcirculatory blood flow induced by motor activity during awake craniotomy," *Neurosurgery,* vol. 118, no. 2, pp. 280-286, 2013.

[67] A. B. Parthasarathy, E. L. Weber, L. M. Richards, D. J. Fox and A. K. Dunn, "Biomedical Optics," vol. 15, no. 6.

[68] N. Hecht, J. Woitzik, J. P. Dreier and P. Vajkoczy, "Intraoperative monitoring of cerebral blood flow by laser speckle contrast analysis," *Neurosurgical Focus,* vol. 27, no. 4, 2009.

[69] A.I. Srienc, Z. L. Kurth-Nelson and E. A. Newman, "Imaging retinal blood flow with laser speckle flowmetry," *Frontiers in Neuroenergetics,* vol. 2, pp. 1-10, 2010.

[70] J. D. Briers and A. F. Fercher, "Retinal blood-flow visualization by means of laser speckle photography," *Investigative Ophthalmology Visual Science,* vol. 22, no. 2, pp. 255-259, 1982.

[71] B. Choi, N. M. Kang and J. S. Nelson, "Laser speckle imaging for monitoring blood flow dynamics in the in vivo redent dorsal skin fold model," *Microvascular Research,* vol. 68, pp. 143-146, 2004.

[72] K. W. a. F. Fobbe, Ed., Color Duplex Sonography: Principles and Clinical Applications, Thieme, 1995.

[73] J. A. Schwarz, C. I. Contescu, and K. Putyera, Dekker Encyclopedia of Nanoscience and Nanotechnolog, vol. 5, CRC Press, 2004.

[74] A. H. Hielscher, J. R. Mourant, and I. J. Bigio, "Influence of particle size and concentration on the diffuse backscattering of polarized light from tissue phantoms and biological cell suspensions," *Applied Optics,* vol. 36, no. 1, pp. 125-135, 1997.